Identification of p38 MAPK and JNK as new targets for correction of Wilson disease-causing ATP7B mutants

Giancarlo Chesi[1], Ramanath N. Hegde[2,#], Simona Iacobacci[1,#], Mafalda Concilli[1,#], Seetharaman Parashuraman[2], Beatrice Paola Festa[1], Elena V. Polishchuk[1], Giuseppe Di Tullio[1], Annamaria Carissimo[1], Sandro Montefusco[1], Diana Canetti[3], Maria Monti[3], Angela Amoresano[3], Piero Pucci[3], Bart van de Sluis[4], Svetlana Lutsenko[5], Alberto Luini[2,*], Roman S. Polishchuk[1, *]

[1] Telethon Institute of Genetics and Medicine, Pozzuoli, Italy

[2] Institute of Protein Biochemistry, National Research Council, Naples, Italy

[3] CEINGE and Department of Chemical Sciences, Federico II University, Naples, Italy

[4] Molecular Genetics Section of Department of Pediatrics, University of Groningen, University Medical Center Groningen, Groningen, The Netherlands

[5] Department of Physiology, Johns Hopkins University, Baltimore, MD, USA

Key Words: Wilson disease - ATP7B mutants – ER quality control - copper homeostasis

Running Title: p38 and JNK suppression allows rescue of ATP7B mutants

FOOTNOTE PAGE

Contact Information. *Roman Polishchuk (polish@tigem.it), Telethon Institute of Genetics and Medicine (TIGEM), Via Campi Flegrei 34, Pozzuoli (NA), 80078, Italy; * Albero Luini, IBP CNR, Via Pietro Castellino 111, Naples, Italy

Authors contribution: # RH, SI and MC contributed equally to the paper.

Abbreviations. WD - Wilson disease, MAPK - mitogen-activated protein kinase, JNK - c-Jun N-terminal kinases, ER – endoplasmic reticulum, ERAD - ER-associated protein degradation, CFTR - cystic fibrosis transmembrane conductance regulator, ROS - reactive oxygen species, PM – plasma membrane, BCS - bathocuproine disulphonate, CS3 - copper sensor 3, ERES - ER export sites, EM – electron microscopy.

Financial Support. This work was supported by grants from Telethon (TGM11CB4 to RP, TGM11CB5 to AL), AIRC (to RP and AL) and MIUR (FaReBio, PON01–00117, PON01–00862, PON03–00025, EPIGEN and Invecchiamento to AL).

ABSTRACT

Wilson disease (WD) is an autosomal recessive disorder that is caused by the toxic accumulation of copper (Cu) in the liver. The *ATP7B* gene, which is mutated in WD, encodes a multi-transmembrane domain ATPase that traffics from the trans-Golgi network (TGN) to the canalicular area of hepatocytes, where it facilitates excretion of excess Cu into the bile. Several *ATP7B* mutations, including H1069Q and R778L that are two of the most frequent variants, result in protein products, which, although still function remain in the endoplasmic reticulum (ER). Thus, they fail to reach Cu excretion sites, resulting in the toxic build-up of Cu in the liver of WD patients. Therefore, correcting the location of these mutants, by leading them to the appropriate functional sites in the cell, should restore Cu excretion and would be beneficial to help large cohorts of WD patients. However, molecular targets for correction of ER-retained ATP7B mutants remain elusive. Here we show that expression of the most frequent ATP7B mutant, H1069Q, activates p38 and JNK signaling pathways, which favor the rapid degradation of the mutant. Suppression of these pathways with RNAi or specific chemical inhibitors results in the substantial rescue of $ATP7B^{H1069Q}$ (as well as that of several other WD-causing mutants) from the ER to the TGN compartment, in recovery of its Cu-dependent trafficking and in reduction of intracellular Cu levels.

CONCLUSION: In summary, our findings indicate p38 and JNK as intriguing targets for correction of WD-causing mutants and, hence, as potential candidates, which could be evaluated for the development of novel therapeutic strategies to combat WD.

INTRODUCTION

The liver is essential for the maintenance of copper (Cu) homeostasis, as it plays a central role in the excretion of this essential, yet toxic, metal. This is highlighted by Wilson disease (WD), an autosomal recessive disorder in which biliary excretion of Cu is severely impaired causing the toxic accumulation of the metal in the liver (1, 2).

The *ATP7B* gene (defective in WD) encodes a Cu-transporting P-type ATPase that pumps cytosolic Cu across cellular membranes, using the energy derived from ATP hydrolysis (Fig. 1A). Increased Cu levels prompt ATP7B to traffic from the Golgi to compartments that are involved in Cu excretion (3, 4). WD-associated mutations affect the intracellular trafficking of ATP7B to the canalicular area of hepatocytes and/or the protein's ability to transfer Cu across the membrane (3, 4). This results in the failure of hepatocytes to remove excess Cu into the bile and, thus, lead to the accumulation of the metal, which causes cell death and Cu accumulation in extra-hepatic tissues. Therefore, clinical features of WD often include hepatic abnormalities, neurological defects, and psychiatric symptoms. When left untreated, liver failure may result in death (1, 2).

WD treatment may be successfully approached with zinc salts and Cu-chelating agents. However, these treatments do have serious toxicities (2, 5). Moreover, about one-third of WD patients do not respond efficiently either to Zn or to Cu chelators (6). All considered, developing novel WD treatment strategies has become an important goal. When approaching therapy solutions, properties of WD-causing mutants should be carefully considered. The most frequent *ATP7B* mutations (Fig. 1A), H1069Q (40%-75% in the white patient population) and R778L (10%-40% of Asian patients), result in ATP7B proteins with significant residual activities (7-9), which, however, are strongly retained in the endoplasmic reticulum (ER) (10). Notably, many other WD-causing ATP7B mutants with substantial Cu-translocating activity undergo complete or partial arrest in the ER (11). Thus, although potentially able to transport Cu, these ATP7B mutants cannot reach the Cu excretion sites to remove excess Cu from hepatocytes. ER retention of such ATP7B mutants occurs due to their mis-folding (10, 11) and increased aggregation (12),

and hence due to their failure to fulfill the requirements of the ER quality control machinery. As a result, the cellular proteostatic network recognizes ATP7B mutants as defective and directs them towards the ER-associated protein degradation (ERAD) pathway (9). Therefore, identifying molecular targets for the recovery of partially- or fully-active ATP7B mutants from the ER to the appropriate functional compartment(s) would be beneficial for the majority of WD patients.

Here we demonstrate, by using both systems biology and classical approaches, that the degradation of the most frequent ATP7B^{H1069Q} mutant is under the control of the stress kinases p38 and JNK. Suppressing both p38 and JNK resulted in the efficient correction of the mutant, thus allowing it to be transported from the ER to the TGN, and supported its Cu-induced trafficking to the post-Golgi vesicles and canalicular surface of polarized hepatic cells. As a consequence, treatments with p38 or JNK inhibitors reduced Cu accumulation in cells expressing ATP7B^{H1069Q} and attenuated degradation of the mutant due to its improved sorting from the ER into the secretory pathway. Our findings suggest that p38 and JNK signaling pathways may serve as attractive targets for the correction of WD-causing mutants and could be explored for the development of therapeutic approaches that counteract WD.

MATERIALS AND METHODS

Antibodies, reagents and DNAs

Antibodies against phospho-p38, phospho-JNK, phospho-ERK, p38, JNK and ERK were Cell Signaling Technology (Beverly, MA, USA). The DNAs of ATP7A and its mutants were already reported (13). DNAs of flag-tagged MKK3, 4, 6 and 7 were obtained from Addgene (Cambridge MA, USA). To obtain the R778L, D765N, L776V, A874V and L1083F mutants of ATP7B, the pEGFPC1-ATP7B construct was used as a template and site-direct mutagenesis was performed according to the manufacturer instructions using the QuickChange kit (Stratagene, La Jolla, CA, USA). Other reagents, antibodies, DNAs and viruses were reported before (14).

Cell culture

HeLa, HepG2 cells and primary mouse hepatocytes were grown in Dulbecco's Modified Eagle's medium (DMEM) supplemented with FCS 10% (decomplemented for HepG2 cells), L-glutamine and Penicillin/Streptomycin.

Immunoprecipitation and mass spectrometry analysis

To compare interactomes of ATP7B^{H1069Q}-GFP or ATP7B^{WT}-GFP, the tagged proteins were immunoprecipitated from cell lysates with the anti-GFP antibody. Pull downs were fractionated by SDS-PAGE and the protein bands were digested with trypsin. Peptide mixtures were analyzed by nano-chromatography tandem mass spectrometry (nanoLC–MS/MS) on a CHIP MS Ion Trap XCT Ultra (Agilent Technologies, Palo Alto, CA, USA). Peptide analysis was performed using data-dependent acquisition of one MS scan (mass range from 400 to 2000 m/z) followed by MS/MS scans of the three most abundant ions in each MS scan. Raw data from nano LC–MS/MS analyses were employed to query a non-redundant protein database using in house MASCOT software (Matrix Science, Boston, USA).

Microarray analysis

To identify the effects of ATP7B^{H1069Q} expression on the transcriptome, total RNA was extracted from HepG2 cells (expressing either ATP7B^{H1069Q}-GFP or ATP7B^{WT}-GFP) and hybridized on Affymetrix GeneChips. All of the raw microarray data was formatted for 'Gene Expression Omnibus' (GEO) to comply with Minimum Information About a Microarray Experiment (MIAME) and Microarray Gene Expression Database (MGED) group standards (GEO number GSE51818). Microarray analyses were carried out with R, a free software environment. Genes that passed all filtering criteria were entered into the DAVID Gene Functional Annotation Tool. The gene ontology options GOTERM_BP_ALL and GOTERM_MF_ALL were selected and a functional annotation chart was generated. A maximum p value of 0.05 was chosen to select only the significant categories.

Statistical analysis

Data were expressed as mean values ± standard deviation. The Student t-test was used to compare differences between two groups by GraphPad Prism 6 software (GraphPad Prism Inc., San Diego, CA, USA). Statistical significant differences between them are indicated by the following asterisks: * $p < 0.05$; ** $p < 0.01$; and *** $p < 0.001$.

Other methods

Adenoviral and VSV infection, DNA transfection, RNA interference, Q-PCR, fluorescent microscopy, immuno-EM, ICP-MS and Western blot analysis were done as previously reported (14). For details see Supplementary Materials.

RESULTS

Expression of the ATP7B^{H1069Q} mutant induces activation of p38 and JNK

We utilized unbiased approaches to understand which molecular pathway could be targeted to correct mutants causing WD. We first sought to determine how ATP7B^{H1069Q} mutant expression affects the transcriptome of hepatic cells. The comparison of microarrays from ATP7B^{H1069Q}- or ATP7B^{WT}-expressing cells revealed 626 differently expressed genes (GSE51818). Gene ontology (GO) analysis of these hits indicated enrichment in genes that regulate cell death and response to stress (Fig. 1B; Supplementary table 1). Several of these genes (SQSTM1, TXNIP, IL6R, FOSL1, MAP2K6 and NET1) have been reported to operate in MAPK signaling pathways mediated by two pro-apoptotic stress kinases, p38 and JNK (15). This might be linked to WD pathogenesis because reactive oxygen species (ROS) accumulating in WD (3) can stimulate the activity of p38 and JNK (15-18). Indeed, several ROS-sensitive genes (SOD2, MSRA, TP53I3) were up-regulated in ATP7B^{H1069Q}-expressing cells. This prompted us to investigate whether the activity of these kinases rises upon ATP7B^{H1069Q} expression. Western blot analysis revealed that phosphorylated p38 and JNK increased significantly in cells expressing the mutant (Fig. 1C), indicating that both kinases were activated. In the mean time the MEK/ERK pathway of the MAPK signaling cascade was not activated, as the levels of phosphorylated ERK remained unaltered in mutant-expressing cells (Fig. S1A).

We also compared the interactomes of ATP7B^{WT} and ATP7B^{H1069Q}. Proteomics analysis revealed 31 ATP7B^{WT}-specific and 51 ATP7B^{H1069Q}-specific interactors (Supplementary tables 2 and 3). GO analysis indicated that specific binding partners of ATP7B^{WT} were enriched in "intracellular trafficking" proteins (Fig. 1D). In contrast, the ATP7B^{H1069Q} interactome contained numerous proteins belonging to the "unfolded protein binding", "proteasome" and "ubiquitination" GO categories (Fig. 1D). These differences are in line with an enhanced association of the mutant with the components of the ER-associated quality control machinery, resulting in ER retention of the mutant (9, 10). Notably, specific MAPK pathways, which include p38 and JNK, have recently been shown to affect proteostasis of proteins such as CFTR (19) and to regulate the expression of ER quality control/degradation genes (15). We thus examined whether the activation of p38 and JNK might lead to the accelerated degradation of ATP7B^{H1069Q}. Indeed, overexpression of the upstream activators of p38 (MKK3 and MKK6) or JNK (MKK4 and MKK7) reduced ATP7B^{H1069Q} levels, indicating increased mutant degradation (Fig. 1E).

On the whole, the above observations indicate that induction of p38 and JNK may be triggered by ATP7B^{H1069Q} expression. This activation, in turn, may promote ER retention and degradation of the mutant, increase in ROS levels (due to Cu accumulation) and further perturbation of ER proteostasis, generating a vicious circle (Fig. 1F). In this context, p38 and JNK represent regulatory centerpieces and potential druggable targets to prevent ER retention of the mutant and, hence, to rescue its localization and function.

Suppression of p38 and JNK rescues appropriate localization and trafficking of the ATP7B^{H1069Q} mutant

To test whether deactivating p38 and JNK pathways facilitates ATP7B^{H1069Q} export from the ER, we suppressed the activity of p38 and JNK first by using specific chemical inhibitors, SB202190 (SB90) and SP600125 (SP125), and then by RNAi. We initially evaluated the impact of p38/JNK-specific inhibitors and siRNAs in HeLa cells, given that the silencing of the genes of interest can be easily achieved in this cell type. In cells

treated with Cu chelator BCS, ATP7B^{WT} was mainly detected over the Golgi membranes, while ATP7B^{H1069Q} remained in the ER (Fig. 2A, upper row). Both p38 and JNK inhibitors (added for 24h) did not affect ATP7B^{WT} (Fig. S2A) but reduced ATP7B^{H1069Q} within the ER and improved the delivery of the mutant to the Golgi (Fig. 2A, upper row; Fig. 2B). The correction of ATP7B^{H1069Q} localization was remarkably effective even at quite low concentrations (Fig. S2B). Interestingly, the combination of p38 and JNK inhibitors did not further increase mutant relocation from the ER to the Golgi (Fig. S3), suggesting that both inhibitors target similar molecular pathways for correction of ATP7B^{H1069Q}. In control experiments the ERK inhibitor failed to correct the mutant from the ER to the Golgi (Fig. S1B). This indicates that only p38 and JNK branches of the MAPK signaling cascade are involved in mutant retention in the ER. Importantly, acute suppression of p38 and JNK did not impact ER export of ATP7B^{H1069Q} (Fig. S4). Therefore, inhibitors apparently act through the transcriptional regulation of quality control and/or trafficking genes rather than by reducing the direct phosphorylation of the mutant or components of its trafficking machinery.

Next, we investigated whether the inhibitors rescue Cu-responsive trafficking of ATP7B^{H1069Q}. $CuSO_4$ addition induced redistribution of ATP7B^{WT} from the TGN to the plasma membrane (PM) and peripheral vesicular structures but failed to induce ATP7B^{H1069Q} relocation from the ER (Fig. 2A, lower row). Instead, when corrected by p38/JNK antagonists, ATP7B^{H1069Q} efficiently moved from the Golgi to the PM and vesicles in response to elevated Cu (Fig. 2A, C).

The above results were confirmed by biochemistry and electron microscopy (EM). Western blot exhibited reduced amounts of ATP7B^{H1069Q} in the PM subcellular fractions in comparison to ATP7B^{WT}, while both p38 and JNK inhibitors significantly increased quantities of the mutant delivered to the cell surface (Fig. S5). In turn, EM revealed ATP7B^{H1069Q} mainly over the ER membrane profiles, while cells incubated with p38 antagonists contained the mutant in TGN membranes (Fig. 2D). In response to $CuSO_4$ treatment inhibitor-treated cells delivered ATP7B^{H1069Q} from the TGN to the cell surface and endosome/lysosome-like “vesicles” (Fig. 2D), which normally receive ATP7B^{WT}

upon Cu overload (14). Thus, it turns out that, once corrected to the Golgi by p38/JNK inhibitors, the mutant reacts to increasing Cu by trafficking to Cu excretion sites, just as ATP7B^{WT} does.

To further verify the above conclusions, we silenced different isoforms of p38 (MAPK11-MAPK14) and JNK (MAPK8-MAPK10) in cells expressing ATP7B^{H1069Q} (Fig. 3A). Both reduction in ER retention and recovery of Golgi and vesicle targeting of the mutant were detected after depletion of MAPK8, MAPK11 and MAPK14 (Fig. 3B, C). In addition, we sought to suppress MAP3K11, the upstream activator of both p38 and JNK (20), to evaluate whether this treatment improved ATP7B^{H1069Q} recovery from the ER. MAP3K11 has been reported to effectively correct Δ508-CFTR (19). Indeed, depletion of MAP3K11 resulted in the strong reduction of ATP7B^{H1069Q} in the ER (Fig. 3B, C).

We next investigated whether inhibitors of p38 or JNK overcome the ER retention of other ATP7B mutants with residual activity (7, 11). Correction was achieved for D765N, L776V and R778L mutants, but not for A874V and L1083F variants (Fig. 4). Meanwhile, p38 and JNK antagonists failed to correct ATP7A mutants with post-Golgi trafficking defects (Fig. 5) indicating that inhibitors act mainly at the ER level. In summary, our observations suggest that suppressing p38 or JNK allows various ATP7B mutants to escape ER retention in a manner that depends on the type of mutation.

p38 and JNK inhibitors rescue ATP7B^{H1069Q} trafficking and targeting in hepatic cells

As a further step, we tested whether suppressing p38 and JNK is efficient in rescuing the mutant in WD-relevant cellular systems such as HepG2 cells and primary hepatocytes (21). In HepG2 cells, ATP7B^{WT} moved from the Golgi to the vesicles and cell membrane in response to Cu (Fig. 6A), while most of the ATP7B^{H1069Q} was arrested in the ER, regardless of changes in Cu concentrations (Fig. 6A). However, incubation with either p38 or JNK inhibitors allowed significant amounts of ATP7B^{H1069Q} to reach the Golgi and to be transported towards the PM and associated vesicles in response to Cu overload

(Fig. 6A, B). Moreover, the ATP7B^{H1069Q} mutant was targeted to the appropriate canalicular surface domain in polarized HepG2 cells (Fig. S6). Importantly, primary hepatocytes exhibited a similar response to either p38 or JNK inhibitors, which rescued ATP7B^{H1069Q} from the ER, and allowed it to traffic towards Golgi and post-Golgi Cu excretion sites (Fig. 6C, D). Therefore, hepatic cells tend to deliver the ATP7B mutant to the right compartments upon suppression of p38 and JNK signaling pathways.

Correction of the ATP7B^{H1069Q} mutant with p38 or JNK inhibitors facilitates Cu excretion

We reasoned that correcting ATP7B^{H1069Q} from the ER to the appropriate Cu excretion sites should reduce the total amount of intracellular Cu. To test this hypothesis we utilized inductively coupled plasma mass spectrometry (ICP-MS). ICP-MS measurements revealed higher concentrations of the metal in the cells expressing ATP7B^{H1069Q}, while treatment with p38 or JNK inhibitor significantly reduced intracellular Cu levels (Fig. 7A).

To further support these findings, we utilized Coppersensor 3 (CS3), which becomes fluorescent in the presence of bioavailable Cu (22). We found low CS3 signal in cells expressing ATP7B^{WT}, whereas CS3 fluorescence was higher in mutant-expressing cells (Fig. 7B). p38 or JNK inhibitors significantly decreased CS3 signal in cells expressing ATP7B^{H1069Q} (Fig. 7B, C). More importantly, reduction in CS3 fluorescence (and hence in Cu levels) correlated to the amount of ATP7B^{H1069Q} expressed in inhibitor-treated cells (Fig. S7). Collectively, the above findings indicate that correcting the mutant to the appropriate compartments with p38/JNK antagonists allows the cells to eliminate excess Cu.

p38 and JNK inhibitors reduce degradation of ATP7B^{H1069Q} by improving mutant sorting into the secretory pathway

In the ER the failure of mis-folded protein to pass the quality control check directs such protein to degradation (23). Therefore, we analyzed whether p38 or JNK inhibitors counteract ATP7B^{H1069Q} degradation. We found that the ATP7B^{H1069Q} protein product

increased in response to p38 and MAPK inhibition (Fig. 8A), while the levels of its mRNA remained the same in treated cells (not shown). This indicated that suppressing p38 and JNK attenuates degradation of the mutant. To support this conclusion we treated cells with cycloheximide and found that p38 and JNK inhibitors significantly slowed down the kinetics of mutant turnover (Fig. 8B, C). Thus, our results suggest that suppression of p38 and JNK pathways allows ATP7B^{H1069Q} to circumvent ER-associated degradation.

How do p38 and JNK antagonists suppress ATP7B^{H1069Q} degradation? The first possibility is that they directly inhibit the ERAD components that comprise the proteasome (23). Being protected from ERAD, aberrant ATP7B molecules would reside in the ER longer and, therefore, may have a higher chance to be incorporated into carriers that transport them from the ER to the Golgi. To test whether this is the case, we treated ATP7B^{H1069Q}-expressing cells with proteasome inhibitor MG132. MG132 increased ATP7B^{H1069Q} levels (Fig. 8D) but failed to overcome mutant retention in the ER (Fig. 8E). This indicates that inhibitor-mediated recovery of ATP7B^{H1069Q} from the ER does not involve ERAD components.

Therefore, ATP7B^{H1069Q} may be protected from the degradation as a result of accelerated trafficking from the ER. To verify this we first observed whether p38 and JNK inhibitors accelerated overall trafficking rates in the secretory pathway. This was not the case as trafficking kinetics of generic cargo protein VSVG was not altered in SB90- or SP125-treated cells (Fig. S8).

We further hypothesized that the suppression of p38 and JNK might specifically accelerate trafficking rates of the ATP7B^{H1069Q} mutant from the ER to the Golgi. To test this hypothesis we used a selective photo-bleaching, which allows to analyze protein exchange between different compartments in live cells (24). We bleached ATP7B^{WT}-GFP or ATP7B^{H1069Q}-GFP in the Golgi region and observed how the material from the ER recovered GFP signal in the bleached area (Fig. 8F). Recovery of ATP7B^{H1069Q}-GFP fluorescence in the Golgi reached the plateau with the same dynamics ($t_{1/2}$≈1 min) both in

control and inhibitor-treated cells (Fig. 8G). However, the amount of ATP7B^{H1069Q}-GFP that reappeared within the Golgi over the same time interval was markedly higher in cells incubated with p38 or JNK inhibitors (Fig. 8F, G). These observations indicate that suppressing p38 and JNK does not shorten the time needed for a given ATP7B^{H1069Q} molecule to be transported from the ER to the Golgi. Instead, p38 and JNK antagonists allow a higher number of ATP7B^{H1069Q} molecules to be sorted from the ER and transported to the Golgi during this interval.

To further support this point we evaluated the distribution of ATP7B^{H1069Q} at the ER export sites (ERES) using immuno-EM. ERES contains coated buds (Fig. 8H-J, arrowheads) emerging from the ER cisternae and associated vesicular-tubular membranes (Fig. 8H-J, empty arrows) that carry newly synthetized proteins to the Golgi. Normally, membrane proteins directed into the secretory pathway (like ATP7B^{WT}) undergo enrichment in the ERES membranes (Fig. 8H, empty arrows) over regular ER cisternae (25). Such concentration in ERES was not detected for ATP7B^{H1069Q}. Indeed, ATP7B^{H1069Q}–associated gold particles decorated mainly ER cisternae (Fig. 8I, arrows) and were scarce in the coated buds (Fig. 8I, arrowhead) and neighboring vesicles (Fig. 8I, empty arrows). Incubation with either p38 or JNK inhibitor increased the density of ATP7B^{H1069Q} in the ERES buds (Fig. 8J, arrowhead) and vesicular profiles (Fig. 8J, empty arrows) and reduced ATP7B^{H1069Q} signal in ER cisternae (Fig. 8J, arrows; quantification in Fig. 8H). This trend indicates that inhibiting p38 and JNK facilitates sorting of ATP7B^{H1069Q} from the ER into nascent Golgi-directed transport intermediates.

DISCUSSION

The main finding in this study is that p38 and JNK kinases play an important role in WD by promoting retention and degradation of the ATP7B^{H1069Q} mutant in the ER. Thus, suppression of p38 and JNK allows ATP7B^{H1069Q} to reach the post-Golgi vesicles and the apical surface in hepatocytes, from where it can contribute to the removal of excess Cu from the cell. As a consequence, treatments with p38 or JNK inhibitors reduce Cu accumulation in cells expressing ATP7B^{H1069Q}. Thus, p38 and JNK represent attractive

targets for correction of the ATP7B mutant localization and function and could be considered for the development of novel therapeutic strategies to counteract WD.

A large proportion of WD-causing *ATP7B* mutations result in a protein product that is still able to pump Cu, but remains retained within the ER, and undergoes accelerated degradation. Therefore, a therapeutic strategy that can target the proteostasis of these ATP7B mutants to reduce their degradation and to improve their folding and export would be beneficial for the large cohort of WD patients.

In recent years, several attempts have been made in this direction, with the use of correctors such as curcumin and phenylbutyrate (9). The rationale for using these drugs is that they are effective in rescuing misfolded CFTR or lysosomal enzymes (26, 27), which result in cystic fibrosis and lysosomal storage diseases, respectively. These drugs were shown to reduce the degradation of several ER-retained mutants of ATP7B (9). Whether and how these correctors rescue the appropriate localization of these ATP7B mutants and, therefore, recover the ability of these aberrant ATP7B proteins to eliminate Cu remains to be demonstrated.

Several proteins have also been reported to modulate the degradation of the ATP7B mutants and/or their retention in the ER. These include COMMD1 (28), clusterin (29) and CRYAB (12). However, these proteins do not belong to the "druggable" category, and, thus, their potential for the development of drugs to cure WD remains questionable. Instead, both p38 and JNK represent *bona-fide* druggable targets and their inhibitors show high efficiency in rescuing several of these pathogenic ATP7B variants. Their ability to recover ATP7B^{H1069Q} trafficking in primary hepatocytes indicates potential efficacy in the hepatic tissue. This property of p38 and JNK inhibitors is really important for therapy since the number of active compounds, which are effective in immortalized cell lines, frequently fail to provide the same beneficial impact in primary cells or animals (30). Unfortunately an animal model that recapitulates ATP7B^{H1069Q} mutation remains to be developed. Therefore, evaluation of the inhibitor efficiency *in vivo* represents a further challenging and important goal.

Of note, the therapeutic potential of some p38 and JNK antagonists has been explored for the treatment of different disorders. Some p38 and JNK inhibitors have entered phase 2 clinical studies for other disorders (ClinicalTrials.gov identifiers: NCT00316771, NCT00303563, NCT00383188, NCT00620685, NCT00395577, NCT00205478, NCT00390845, NCT00570752, NCT01630252) (31). Thus, in theory the passage of such p38 and JNK inhibitors into clinical use for WD might be rapid, as their toxicity level has reported to be relatively low (32) and may be further decreased through specific delivery using ligands of the asialoglycoprotein receptor (33).

Which molecular mechanisms operate behind the correction of the ATP7B^{H1069Q} mutant? As we have demonstrated, the inhibition of p38 and JNK manifests two main phenomena: a reduction in ATP7B^{H1069Q} degradation and an improved ATP7B^{H1069Q} delivery to the Golgi apparatus and to the post-Golgi compartments. It turns out that a reduction in the degradation of ATP7B^{H1069Q} occurs as a consequence of increasingly efficient sorting of ATP7B^{H1069Q} into the secretory pathway. Indeed, photo-bleaching experiments and immuno-EM indicate that p38 and JNK inhibitors facilitate ATP7B mutant sorting from the ER into the secretory pathway at the level of the ER exit sites, while overall membrane trafficking rates remain unchanged.

Therefore, corrections of ATP7B^{H1069Q} from the ER into the secretory route probably arise through the modulation of the proteostatic network, which improve the ability of ATP7B^{H1069Q} to be captured by the export machinery in inhibitor-treated cells. ATP7B^{H1069Q} interactome exhibits a significant enrichment in components of ER quality control and ERAD. Thus, an excessive amount of quality control proteins that bind the mutant may prevent its transition from the ER to the secretory pathway. Such chaperone-mediated ER trap was reported for CFTR mutant (34). The inhibitors of p38 and JNK might reduce the amounts of quality control proteins that bind the ATP7B mutant and in this way allow ATP7B^{H1069Q} to escape into the secretory pathway.

Alternatively, the inhibition of p38 and JNK may result in the up-regulation of some chaperones that are negatively regulated by these stress kinases. Thus, up-regulation of such chaperones could improve mutant folding and stability in cells treated with p38 or JNK antagonists. We have previously shown that CRYAB chaperone significantly facilitates ATP7B^{H1069Q} exit from the ER (12). Its activity and expression appear to be regulated by p38 (35), and, therefore, might also be modulated by p38 inhibition. It remains to be investigated whether p38 antagonists can induce CRYAB up-regulation in hepatocytes that express ATP7B mutants.

Although p38 and JNK inhibitors were effective in correcting several ER-retained ATP7B variants, they did not rescue a few other ATP7B mutants from the ER. Interestingly, mutations in the same domain (like ATP7B^{H1069Q} and ATP7B^{L1083F}) are differently sensitive to p38 and JNK inhibitors. This indicates that p38-dependent and JNK-dependent machineries have a certain level of specificity and that inhibiting them does not seem to threaten the global quality-control processes at the level of the ER. On the other hand, p38 and JNK inhibitors also rescue some, but not all, ER-retained mutants of other membrane proteins, such as CFTR and P-glycoprotein (19). Therefore, these p38 and JNK inhibitors might modulate specific mechanisms involved in the recognition of common (or similar) protein-folding defects.

In conclusion, p38 and JNK signaling pathways may serve as attractive targets to counteract WD by rescuing ER-retained ATP7B mutants. It remains to be established to what extent suppression of these pathways would be able to prevent toxic copper accumulation in model animals or patients carrying corresponding *ATP7B* mutations. On the other hand, the impact of p38 and JNK antagonists on the key components of proteostatic networks requires further detailed investigation. This may expand the use of kinase inhibitors to correction of other ER-retained pathogenic mutants and, hence, to open new avenues for therapeutic strategies to combat disorders that are caused by protein misfolding.

ACKNOWLEDGEMENTS

We would like to acknowledge those who provided us with antibodies, reagents and cells. Christopher J. Chang and Jefferson Chan for help with CS3, Diego di Bernardo, Fabiana Ciciriello and TIGEM Bioinformatics Core for analysis of proteomics and microarray results, TIGEM Advanced Microscopy and Imaging Core for microscopy support and TIGEM Vector Core for production of adenoviruses.

REFERENCES

1. Gitlin JD. Wilson disease. Gastroenterology 2003;125:1868-1877.
2. Ferenci P. Review article: diagnosis and current therapy of Wilson's disease. Alimentary pharmacology & therapeutics 2004;19:157-165.
3. Lutsenko S, Barnes NL, Bartee MY, Dmitriev OY. Function and regulation of human copper-transporting ATPases. Physiol Rev 2007;87:1011-1046.
4. La Fontaine S, Mercer JF. Trafficking of the copper-ATPases, ATP7A and ATP7B: role in copper homeostasis. Arch Biochem Biophys 2007;463:149-167.
5. Roberts EA, Schilsky ML. Diagnosis and treatment of Wilson disease: an update. Hepatology 2008;47:2089-2111.
6. Iorio R, D'Ambrosi M, Marcellini M, Barbera C, Maggiore G, Zancan L, Giacchino R, et al. Serum transaminases in children with Wilson's disease. Journal of pediatric gastroenterology and nutrition 2004;39:331-336.
7. Forbes JR, Cox DW. Functional characterization of missense mutations in ATP7B: Wilson disease mutation or normal variant? Am J Hum Genet 1998;63:1663-1674.
8. Iida M, Terada K, Sambongi Y, Wakabayashi T, Miura N, Koyama K, Futai M, et al. Analysis of functional domains of Wilson disease protein (ATP7B) in Saccharomyces cerevisiae. FEBS letters 1998;428:281-285.
9. van den Berghe PV, Stapelbroek JM, Krieger E, de Bie P, van de Graaf SF, de Groot RE, van Beurden E, et al. Reduced expression of ATP7B affected by Wilson disease-causing mutations is rescued by pharmacological folding chaperones 4-phenylbutyrate and curcumin. Hepatology 2009;50:1783-1795.
10. Payne AS, Kelly EJ, Gitlin JD. Functional expression of the Wilson disease protein reveals mislocalization and impaired copper-dependent trafficking of the common H1069Q mutation. Proc Natl Acad Sci U S A 1998;95:10854-10859.
11. Huster D, Kuhne A, Bhattacharjee A, Raines L, Jantsch V, Noe J, Schirrmeister W, et al. Diverse functional properties of Wilson disease ATP7B variants. Gastroenterology 2012;142:947-956 e945.
12. D'Agostino M, Lemma V, Chesi G, Stornaiuolo M, Cannata Serio M, D'Ambrosio C, Scaloni A, et al. The cytosolic chaperone alpha-crystallin B rescues folding and compartmentalization of misfolded multispan transmembrane proteins. Journal of cell science 2013;126:4160-4172.
13. Vonk WI, de Bie P, Wichers CG, van den Berghe PV, van der Plaats R, Berger R, Wijmenga C, et al. The copper-transporting capacity of ATP7A mutants associated with Menkes disease is ameliorated by COMMD1 as a result of improved protein expression. Cellular and molecular life sciences : CMLS 2012;69:149-163.

14. Polishchuk EV, Concilli M, Iacobacci S, Chesi G, Pastore N, Piccolo P, Paladino S, et al. Wilson Disease Protein ATP7B Utilizes Lysosomal Exocytosis to Maintain Copper Homeostasis. Developmental cell 2014.
15. Darling NJ, Cook SJ. The role of MAPK signalling pathways in the response to endoplasmic reticulum stress. Biochimica et biophysica acta 2014.
16. Nawaz M, Manzl C, Lacher V, Krumschnabel G. Copper-induced stimulation of extracellular signal-regulated kinase in trout hepatocytes: the role of reactive oxygen species, Ca2+, and cell energetics and the impact of extracellular signal-regulated kinase signaling on apoptosis and necrosis. Toxicol Sci 2006;92:464-475.
17. Chen SH, Lin JK, Liu SH, Liang YC, Lin-Shiau SY. Apoptosis of cultured astrocytes induced by the copper and neocuproine complex through oxidative stress and JNK activation. Toxicol Sci 2008;102:138-149.
18. Rupesh KR, Priya AM, Sundarakrishnan B, Venkatesan R, Lakshmi BS, Jayachandran S. 2,2'-bipyridyl based copper complexes down regulate expression of pro-inflammatory cytokines and suppress MAPKs in mitogen induced Peripheral blood mononuclear cells. Eur J Med Chem 2010;45:2141-2146.
19. Hegde R, Parashuraman S, Iorio F, Capuani F, Ciciriello F, Carissimo A, Carella D, et al. Unravelling druggable signalling networks that control F508del-CFTR proteostasis. Elife (Submitted) 2015.
20. Brancho D, Ventura JJ, Jaeschke A, Doran B, Flavell RA, Davis RJ. Role of MLK3 in the regulation of mitogen-activated protein kinase signaling cascades. Molecular and cellular biology 2005;25:3670-3681.
21. Cater MA, La Fontaine S, Shield K, Deal Y, Mercer JF. ATP7B mediates vesicular sequestration of copper: insight into biliary copper excretion. Gastroenterology 2006;130:493-506.
22. Dodani SC, Domaille DW, Nam CI, Miller EW, Finney LA, Vogt S, Chang CJ. Calcium-dependent copper redistributions in neuronal cells revealed by a fluorescent copper sensor and X-ray fluorescence microscopy. Proceedings of the National Academy of Sciences of the United States of America 2011;108:5980-5985.
23. Vembar SS, Brodsky JL. One step at a time: endoplasmic reticulum-associated degradation. Nature reviews. Molecular cell biology 2008;9:944-957.
24. Polishchuk EV, Di Pentima A, Luini A, Polishchuk RS. Mechanism of constitutive export from the golgi: bulk flow via the formation, protrusion, and en bloc cleavage of large trans-golgi network tubular domains. Mol Biol Cell 2003;14:4470-4485.
25. Bannykh SI, Rowe T, Balch WE. The organization of endoplasmic reticulum export complexes. The Journal of cell biology 1996;135:19-35.
26. Singh OV, Pollard HB, Zeitlin PL. Chemical rescue of deltaF508-CFTR mimics genetic repair in cystic fibrosis bronchial epithelial cells. Mol Cell Proteomics 2008;7:1099-1110.
27. Mu TW, Ong DS, Wang YJ, Balch WE, Yates JR, 3rd, Segatori L, Kelly JW. Chemical and biological approaches synergize to ameliorate protein-folding diseases. Cell 2008;134:769-781.
28. de Bie P, van de Sluis B, Burstein E, van de Berghe PV, Muller P, Berger R, Gitlin JD, et al. Distinct Wilson's disease mutations in ATP7B are associated with enhanced binding to COMMD1 and reduced stability of ATP7B. Gastroenterology 2007;133:1316-1326.

29. Materia S, Cater MA, Klomp LW, Mercer JF, La Fontaine S. Clusterin (apolipoprotein J), a molecular chaperone that facilitates degradation of the copper-ATPases ATP7A and ATP7B. The Journal of biological chemistry 2011;286:10073-10083.
30. Trzcinska-Daneluti AM, Nguyen L, Jiang C, Fladd C, Uehling D, Prakesch M, Al-awar R, et al. Use of kinase inhibitors to correct DeltaF508-CFTR function. Molecular & cellular proteomics : MCP 2012;11:745-757.
31. Damjanov N, Kauffman RS, Spencer-Green GT. Efficacy, pharmacodynamics, and safety of VX-702, a novel p38 MAPK inhibitor, in rheumatoid arthritis: results of two randomized, double-blind, placebo-controlled clinical studies. Arthritis Rheum 2009;60:1232-1241.
32. Kumar S, Boehm J, Lee JC. p38 MAP kinases: key signalling molecules as therapeutic targets for inflammatory diseases. Nat Rev Drug Discov 2003;2:717-726.
33. Pujol AM, Cuillel M, Renaudet O, Lebrun C, Charbonnier P, Cassio D, Gateau C, et al. Hepatocyte targeting and intracellular copper chelation by a thiol-containing glycocyclopeptide. J Am Chem Soc 2011;133:286-296.
34. Wang X, Venable J, LaPointe P, Hutt DM, Koulov AV, Coppinger J, Gurkan C, et al. Hsp90 cochaperone Aha1 downregulation rescues misfolding of CFTR in cystic fibrosis. Cell 2006;127:803-815.
35. Clements RT, Feng J, Cordeiro B, Bianchi C, Sellke FW. p38 MAPK-dependent small HSP27 and alphaB-crystallin phosphorylation in regulation of myocardial function following cardioplegic arrest. Am J Physiol Heart Circ Physiol 2011;300:H1669-1677.

FIGURE LEGENDS

Fig. 1. Expression of the ATP7B^{H1069Q} mutant is associated with activation of p38 and JNK signaling pathways.

(A) Schematic structure of ATP7B. Black balls show N-terminal metal binding domains. Numbers indicate trans-membrane helices. The domains, which regulate ATPase activity, are indicated in italic with D residue for catalytic phosphorylation. Yellow stars indicate the position of the most frequent WD-causing mutations, H1069Q and R778L. **(B)** HepG2 cells were infected with Ad-ATP7B^{WT}-GFP or Ad-ATP7B^{H1069Q}-GFP and prepared for microarray analysis (see Methods). Genes that were differently expressed in cells expressing ATP7B^{H1069Q} were analyzed for gene ontology (GO) enrichment. The pie diagram shows the GO categories that were enriched among the altered genes in ATP7B^{H1069Q}-expressing cells, as opposed to cells expressing ATP7B^{WT} (see also Supplementary table 1). Genes involved in the regulation of apoptosis constituted the largest group of genes, whose expression was altered by the ATP7B^{H1069Q} mutant. **(C)** HepG2 cells were infected with Ad-ATP7B^{WT}-GFP or Ad-ATP7B^{H1069Q}-GFP and analyzed with western blot. Phosphorylated forms of p38 (P-38) or JNK (P-JNK) increased in cells expressing the ATP7B^{H1069Q} mutant, while overall amounts of p38 or

JNK remained similar in WT- and mutant-expressing cells. **(D)** Putative interactors of $ATP7B^{WT}$ and $ATP7B^{H1069Q}$ were identified using a proteomics approach (see Methods). The diagram shows the number of interactors that were specific for $ATP7B^{WT}$ or for $ATP7B^{H1069Q}$, as well as the number of common interactors. GO analysis revealed $ATP7B^{WT}$ interactors to be enriched in proteins belonging to membrane trafficking categories, while mutant-specific interactors were enriched in proteins involved in ER-associated protein quality control and degradation. **(E)** HepG2 cells expressing $ATP7B^{H1069Q}$ were transfected with activators of p38 (MKK3 and MKK6) or JNK (MKK4 and MKK7). Western blot (see also quantification graph) revealed a decrease in $ATP7B^{H1069Q}$ levels in cells expressing p38 or JNK activators. Na/K-ATPase was used as input control. The modest decrease in $ATP7B^{H1069Q}$ in cells transfected with MKK4 is due to lower over-expression of MKK4 in comparison to other MKKs. **(F)** The schematic drawing shows a vicious circle that is generated by expression of the $ATP7B^{H1069Q}$ mutant, which leads to activation of ER quality control and degradation of $ATP7B^{H1069Q}$. As a consequence of $ATP7B^{H1069Q}$ loss, ROS increase and stimulates p38 and JNK signaling which triggers further retention and degradation of the mutant in the ER preventing it from being exported to the secretory pathway.

Fig. 2. Inhibitors of p38 and JNK correct localization and trafficking of $ATP7B^{H1069Q}$ mutant.

(A) HeLa cells were infected with Ad-$ATP7B^{WT}$-GFP or Ad-$ATP7B^{H1069Q}$-GFP, incubated overnight with 200 μM BCS, and fixed or incubated for an additional 2h with 100 μM $CuSO_4$. In response to Cu, $ATP7B^{WT}$ (left column) traffics from the Golgi (arrowheads in upper panel) to the PM and vesicle (arrows in lower panel), while $ATP7B^{H1069Q}$ (second column) is retained within the ER under both low and high Cu conditions. p38 inhibitor SB202190 (5mM) or JNK inhibitor SP600125 (2mM) were added to the cells 24h before fixation (as indicated in the corresponding panels). Fixed cells were further labeled for TGN46 and visualized under a confocal microscope. Both p38 and JNK inhibitors corrected $ATP7B^{H1069Q}$ from the ER to the Golgi (arrowheads in upper panels) under low Cu conditions and to the PM and vesicles (arrows in lower panels) in high Cu conditions. **(B)** Cells were treated with BCS and drugs as shown in panel A. Fluorescence of ATP7B signal in the Golgi (average ± SD, n=40 cells) was quantified and normalized to total cell fluorescence. Both inhibitors caused an increase of $ATP7B^{H1069Q}$ signal in the Golgi region. **(C)** Cells were treated as in panel A. The percentage of cells (average ± SD, n=10 fields) with an ATP7B signal in the ER, Golgi or PM/vesicles was calculated. Both p38 and JNK inhibitors reduced the percentage of cells exhibiting $ATP7B^{H1069Q}$ in the ER and increased the number of cells in which ATP7B was corrected to the Golgi under low Cu conditions and to the PM and vesicles upon Cu stimulation. **(D)** Cells were treated as in panel A and prepared for immuno-EM (see Methods). Arrows indicate $ATP7B^{H1069Q}$ in the ER. Arrowheads show $ATP7B^{WT}$ or

ATP7B^{H1069Q} in the Golgi. Empty arrows indicate ATP7B^{WT} or ATP7B^{H1069Q} signal at the PM, while asterisks label ATP7B-positive MVB-like vesicles. Scale bar: 5 μm (A), 260 nm (D).

Fig. 3. Silencing of several p38 and JNK isoforms corrects localization and trafficking of the ATP7B^{H1069Q} mutant.

(A) HeLa cells were incubated with siRNA, which targets specific genes (indicated in graph) belonging to the p38 and JNK pathways. The efficiency of silencing for each gene was evaluated by quantitative RT-PCR and expressed as fold-change (average ± SD; n=3 experiments) after normalization to mRNA levels of the same gene in control cells (treated with scramble siRNA). **(B)** HeLa cells were silenced for different p38 and JNK isoforms as in panel A, then infected with Ad-ATP7B^{H1069Q}-GFP and incubated for 2h with 100 μM $CuSO_4$. Fixed cells were then labeled for TGN46 and visualized under a confocal microscope. Silencing of MAPK8, MAPK11, MAPK14 or MAP3K11 showed the rescue of ATP7B^{H1069Q} from the ER and its movement to the post-Golgi vesicles (arrows) and PM. **(C)** Cells were treated as in panel B. The percentage of cells (average ± SD, n=10 fields) with ATP7B^{H1069Q} signal in the ER was calculated. RNAi of MAPK8, MAPK11, MAPK14 and MAP3K11 reduced the percentage of cells exhibiting ATP7B^{H1069Q} in the ER. Scale bar: 4.7 μm (B).

Fig. 4. Impact of p38 and JNK inhibitors on localization of ER-retained ATP7B mutants.

(A) HeLa cells were transfected with different ATP7B mutants (indicated in each panel), then treated for 24h with either p38 or JNK inhibitors and exposed to 100 μM $CuSO_4$ for 2h. Cells were then fixed, labeled for TGN46 and visualized under a confocal microscope. All mutants exhibited clear ER patterns in cells that were not treated with inhibitors. Incubation with either p38 or JNK inhibitors allowed R778L, D765N and L776V mutants of ATP7B to be transported to the Golgi, post-Golgi vesicles (arrows) and PM. In contrast, inhibitors did not recover either L1083F or A874V mutants of ATP7B from the ER (two bottom rows). **(B)** Cells were treated as in panel A. The percentage of cells (average ± SD, n=10 fields) with ATP7B signal in the ER was calculated for each mutant. p38 and JNK inhibitors reduced the percentage of cells that exhibited R778L, D765N and L776V in the ER. Scale bar: 5 μm (A).

Fig. 5. p38 and JNK inhibitors do not rescue post-Golgi trafficking of ATP7A mutants.

HeLa cells were transfected with either ATP7A^{WT} (A), ATP7A^{A1362D} (B) or ATP7A^{L873R} (C) mutant. Then the cells were exposed to a 200 μM treatment with BCS (-Cu) and fixed directly or incubated with 100 μM $CuSO_4$ for an additional 2h (+Cu). p38 or JNK inhibitors were added (as indicated in panels B and C) for 24h prior to fixation. Fixed

cells were labeled for TGN46 and visualized under a confocal microscope. **(A)** $ATP7A^{WT}$ moved from the Golgi (top panel) to the PM (bottom panel) after Cu increase. **(B)** $ATP7B^{A1362D}$ mutant remained associated with TGN46 under both low and high Cu conditions (left column). Neither p38 nor JNK inhibitors allowed the mutant to be transported from the Golgi to the PM in response to increasing Cu (middle and right column). **(C)** The $ATP7A^{L873R}$ mutant remained distributed over the PM, independently of the Cu levels (left column). Incubation with p38 or JNK inhibitors did not correct the mutant from the PM to the Golgi (middle and right column), even when Cu levels were low (top row). Scale bar: 4.8 μm (A-C).

Fig. 6. Suppression of p38 and JNK corrects localization and trafficking of $ATP7B^{H1069Q}$ mutant in hepatic cells.

(A) HepG2 cells were infected with Ad-$ATP7B^{WT}$-GFP or Ad-$ATP7B^{H1069Q}$-GFP, incubated overnight with 200 μM BCS, and fixed or incubated for an additional 2h with 100 μM $CuSO_4$. In response to Cu, $ATP7B^{WT}$ (left column) traffics from the Golgi (arrowheads in upper panels) to the PM and vesicles (arrows in lower panels), while $ATP7B^{H1069Q}$ (second column) is retained in the ER under both low and high Cu conditions. p38 or JNK inhibitors were added to the cells 24h before fixation (as indicated in the corresponding panels). Fixed cells were then labeled for TGN46 and visualized under a confocal microscope. Both p38 and JNK inhibitors corrected $ATP7B^{H1069Q}$ from the ER to the Golgi (arrowheads in upper panels) under low Cu conditions and to the PM and vesicles (arrows in lower panels) upon Cu exposure. **(B)** Cells were treated as in panel A. The percentage of cells (average ± SD, n=10 fields) with ATP7B signal in the ER, Golgi or PM/vesicles was calculated. Both p38 and JNK inhibitors reduced the percentage of cells exhibiting $ATP7B^{H1069Q}$ in the ER independently from the Cu levels and increased the number of cells in which ATP7B was corrected to the Golgi under low Cu conditions and to the PM and vesicles upon Cu stimulation. **(C)** Primary hepatocytes isolated from mice liver cells were infected with Ad-$ATP7B^{WT}$-GFP or Ad-$ATP7B^{H1069Q}$-GFP, and then incubated with 100 μM $CuSO_4$ for 2h. p38 or JNK inhibitors were added to the cells 24h before fixation (as indicated in the corresponding panels). Fixed cells were then labeled for giantin and visualized under a confocal microscope. Both p38 and JNK inhibitors corrected $ATP7B^{H1069Q}$ from the ER to the PM and vesicles (arrows). **(D)** Primary hepatocytes were treated as in panel C. The percentage of cells (average ± SD, n=10 fields) with ATP7B signal in the ER, Golgi or PM/vesicles was calculated. Both p38 and JNK inhibitors reduced the percentage of cells exhibiting $ATP7B^{H1069Q}$ in the ER and increased the number of cells in which ATP7B was corrected to the PM and vesicles upon Cu stimulation. Scale bar: 5 μm (A), 5.3 μm (C).

Fig. 7. Inhibitors of p38 and JNK reduce copper levels in cells expressing $ATP7B^{H1069Q}$ mutant.

(A) HepG2 cells were infected with Ad-ATP7B^{WT}-GFP or Ad-ATP7B^{H1069Q}-GFP and incubated with p38 or JNK inhibitor. $CuSO_4$ at 100 μM concentration was added to the cells for the last 2h of incubation with the inhibitors. The cells were examined with ICP-MS (see Methods), which revealed an increase in normalized intracellular Cu levels (average ± SD; n=3 experiments) in ATP7B^{H1069Q}-expressing cells. Both p38 and JNK inhibitors reduced Cu levels in ATP7B^{H1069Q}-expressing cells. **(B)** HepG2 cells were infected with Ad-ATP7B^{WT}-GFP or Ad-ATP7B^{H1069Q}-GFP and incubated for 2h with 100 μM $CuSO_4$ and loaded with CS3 before fixation. p38 or JNK inhibitors were added to the cells 24h before fixation (as indicated in the corresponding panels). Confocal microscopy images show CS3 fluorescence in red (top row), in white (middle row) and in false color scale (bottom row). Cells expressing ATP7B^{H1069Q} exhibited higher CS3 signals than cells expressing ATP7B^{WT}, while both p38 and JNK inhibitors decreased CS3 fluorescence in ATP7B^{H1069Q}-expressing cells. **(C)** Quantification revealed an increase in CS3 fluorescence (average ± SD; n=10 fields) in cells expressing ATP7B^{H1069Q} and a decrease of CS3 signal upon incubation with either p38 or JNK inhibitors. Scale bar: 14 μm (C).

Fig. 8. p38 and JNK inhibitors reduce degradation of ATP7B^{H1069Q} mutant and improve its sorting into the secretory pathway.

(A) HepG2 cells were infected with Ad-ATP7B^{H1069Q} and treated with p38 or JNK inhibitor. Western blot revealed an increase in the amount of ATP7B^{H1069Q} after suppression of p38 or JNK. **(B, C)** HepG2 cells expressing ATP7B^{H1069Q} were treated with p38 and JNK inhibitors and then exposed to 100μM cycloheximide (CHX) for different time intervals. Western blot (B) and quantification of ATP7B^{H1069Q} bands (C) showed a decrease of ATP7B^{H1069Q} signals (means±SD; n=3 experiments) in control cells exposed to CHX, while p38 and JNK inhibitors attenuated the decay of ATP7B^{H1069Q} levels. **(D, E)** HepG2 cells expressing ATP7B^{H1069Q} were treated with 20μM proteasome inhibitor MG132. Although Western blot indicated an increase in ATP7B^{H1069Q} protein levels (D), the localization of the mutant (E) was similar in control and MG132-treated cells. **(F, G)** HeLa cells expressing either ATP7B^{WT}-GFP or ATP7B^{H1069Q}-GFP were observed *in vivo*. p38 or JNK inhibitor was added to some ATP7B^{H1069Q}-GFP-expressing cells 24h before the experiment. The GFP signal within the Golgi area (outlined in red) was photo-bleached (see Methods), and the kinetics of its recovery in the bleached region was analyzed. Both time-lapse images (F) and a kinetics plot (G) revealed more efficient recovery of ATP7B^{WT}-GFP in comparison to the mutant. Incubation with p38 or JNK inhibitor led to recovery of higher ATP7B^{H1069Q}-GFP levels (means±SD; n=6 cells) in the bleached Golgi area (F, G), although the half time ($t_{1/2}$) of the recovery process remained similar in control and treated cells (G). **(H-K)** HepG2 cells expressing ATP7B^{WT}-GFP or ATP7B^{H1069Q}-GFP were fixed and prepared for immuno-EM with anti-GFP antibody. Part of ATP7B^{H1069Q}-GFP-expressing cells was incubated with p38 or JNK inhibitor. ER (arrows), buds (arrowheads) or ERES vesicular/tubular profiles (empty arrows) are

indicated in panels H-J. Panel K shows an increase in normalized density of gold particles associated with ATP7B^{H1069Q}-GFP (means±SD; n=20 ERES) at the ERES structures in inhibitor-treated cells. Scale bar: 6.5 μm (E), 5 μm (F), 180 nm (H-J).

Fig. 1. Chesi et al.

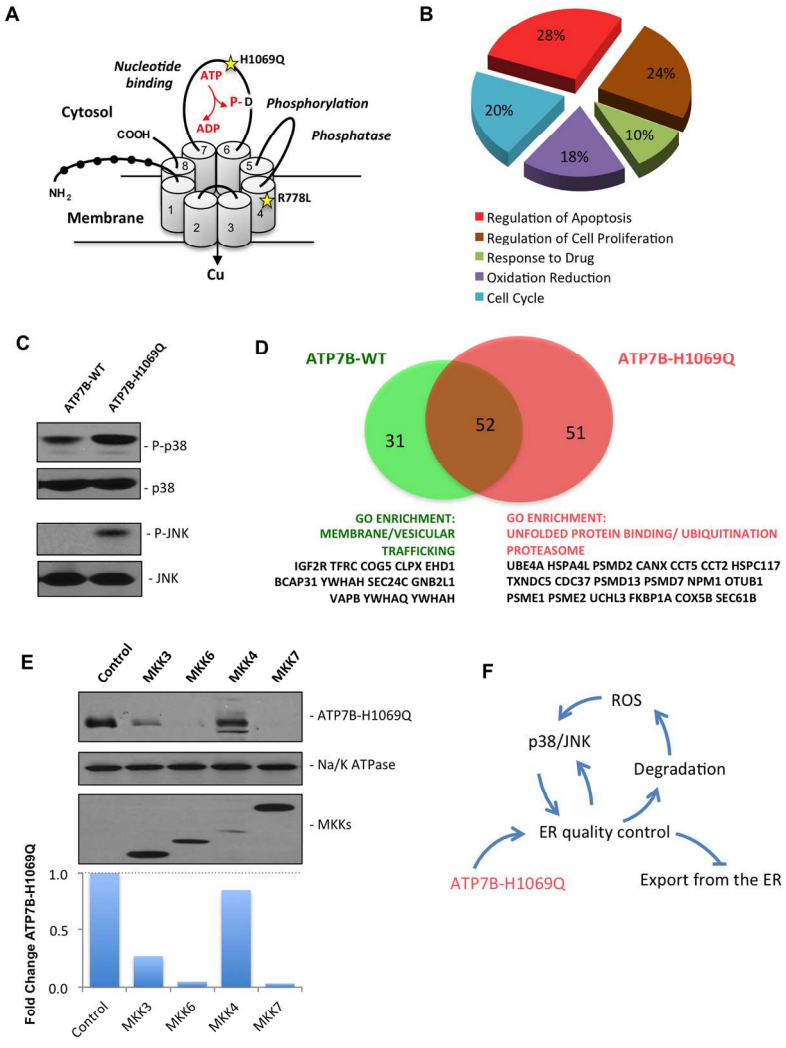

189x253mm (300 x 300 DPI)

Fig. 2. Chesi et al.

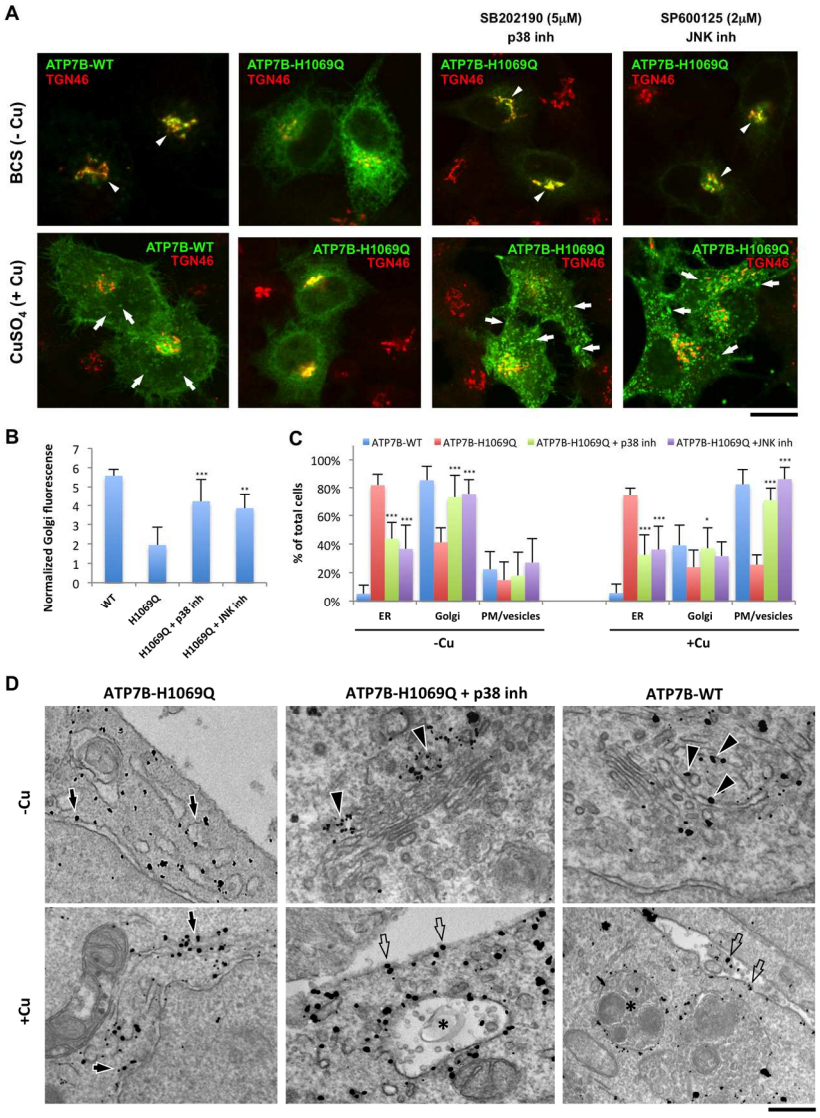

189x253mm (300 x 300 DPI)

Fig. 3 Chesi et al.

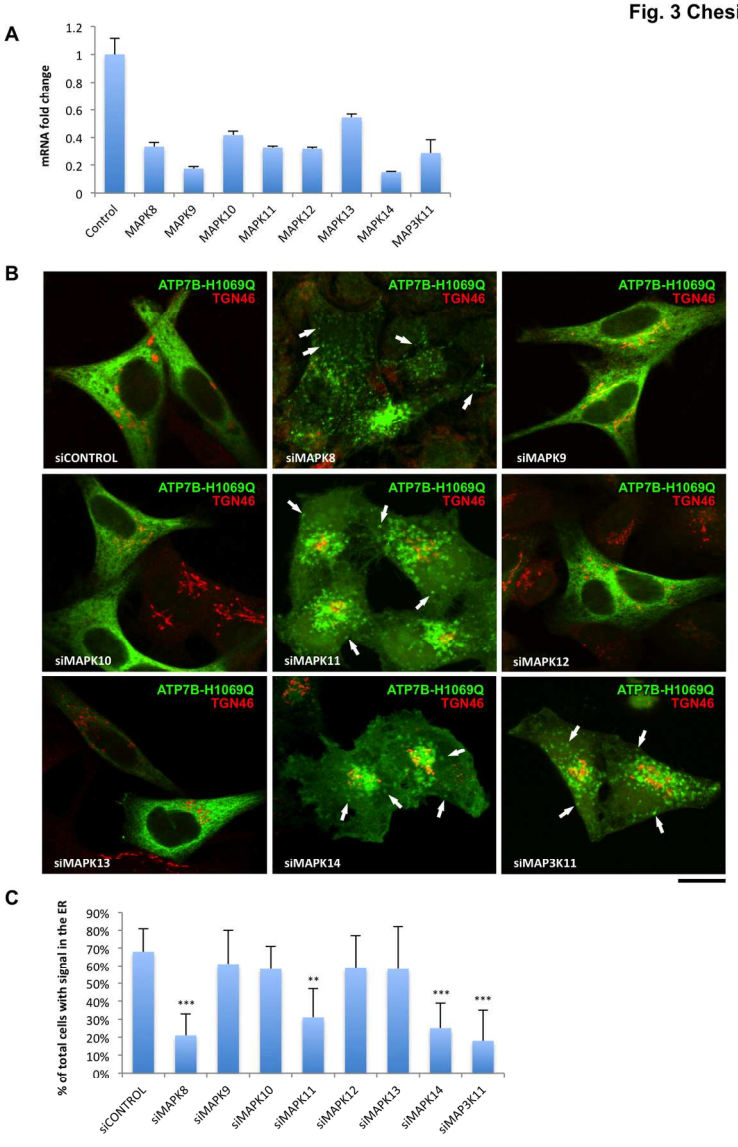

189x253mm (300 x 300 DPI)

Fig. 4. Chesi et al.

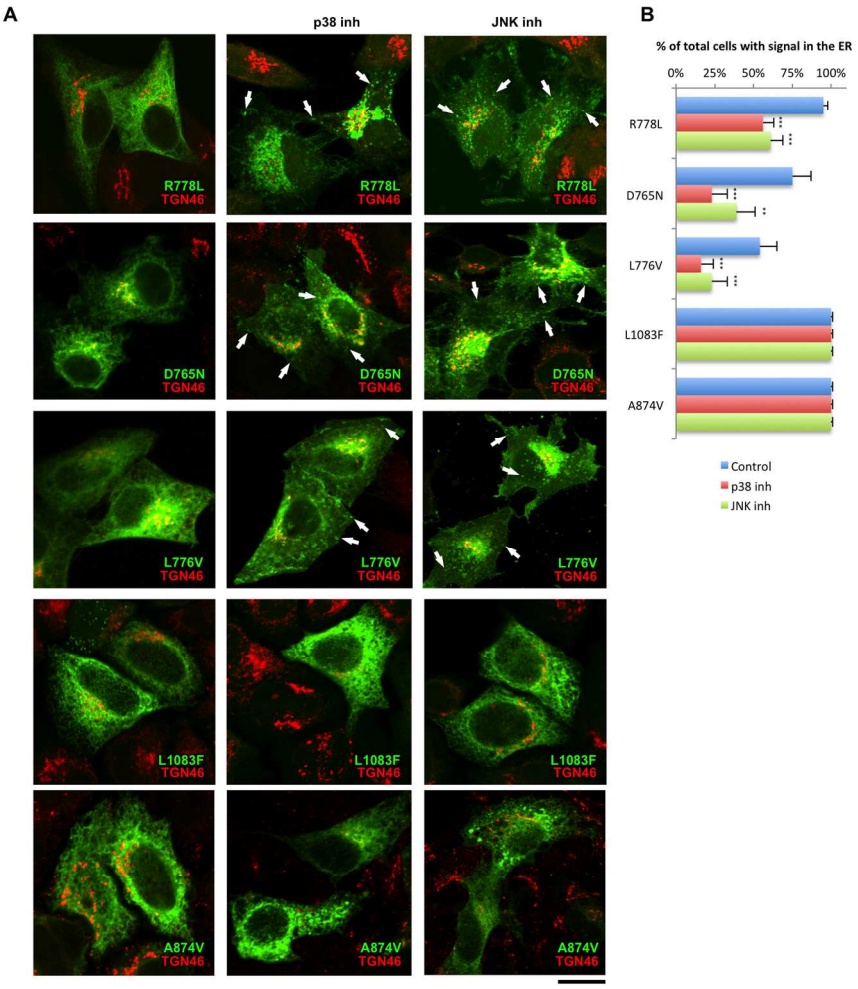

189x253mm (300 x 300 DPI)

Fig. 5. Chesi et al.

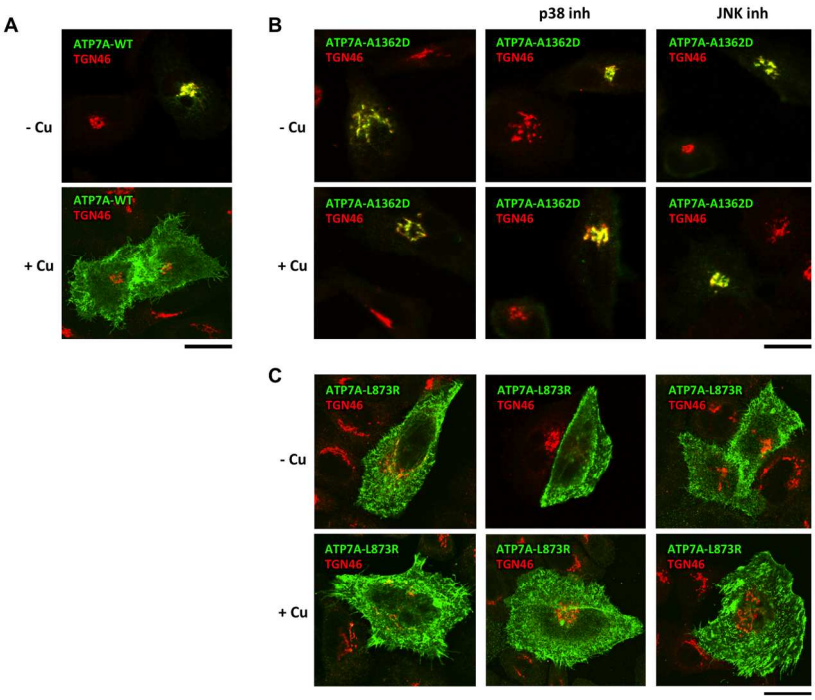

189x253mm (300 x 300 DPI)

Fig. 6. Chesi et al.

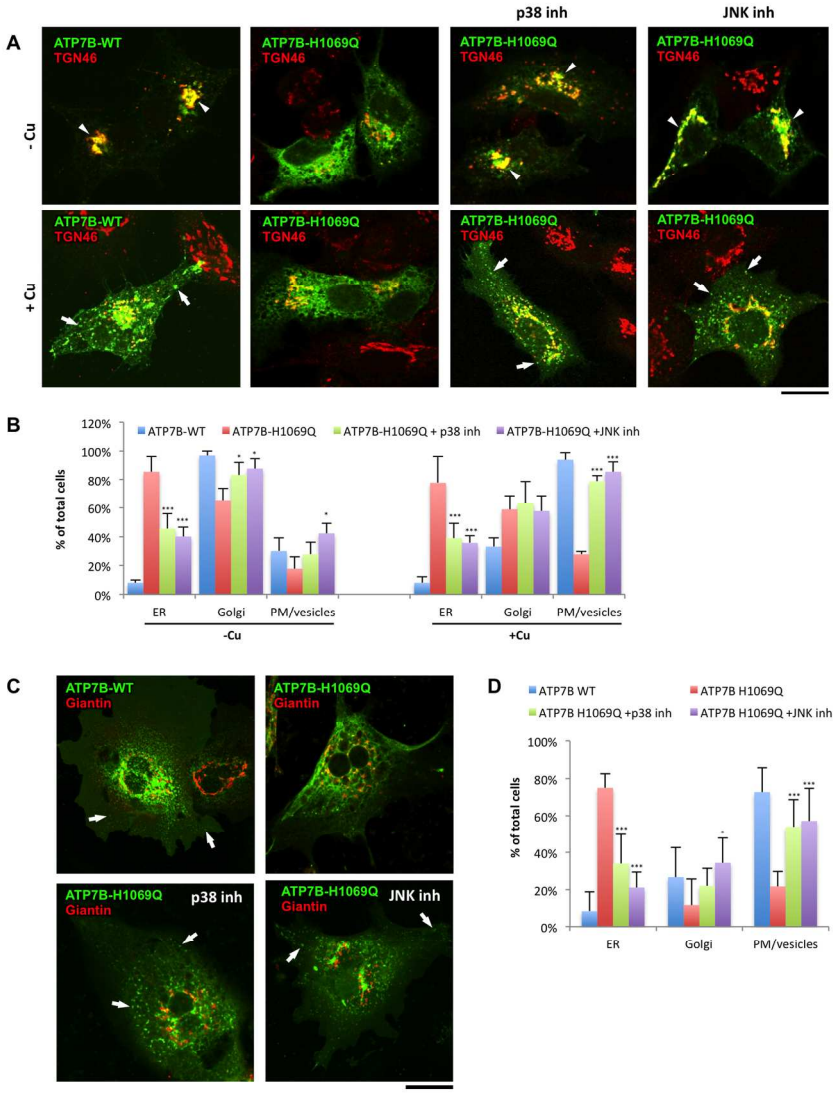

189x253mm (300 x 300 DPI)

Fig. 7. Chesi et al.

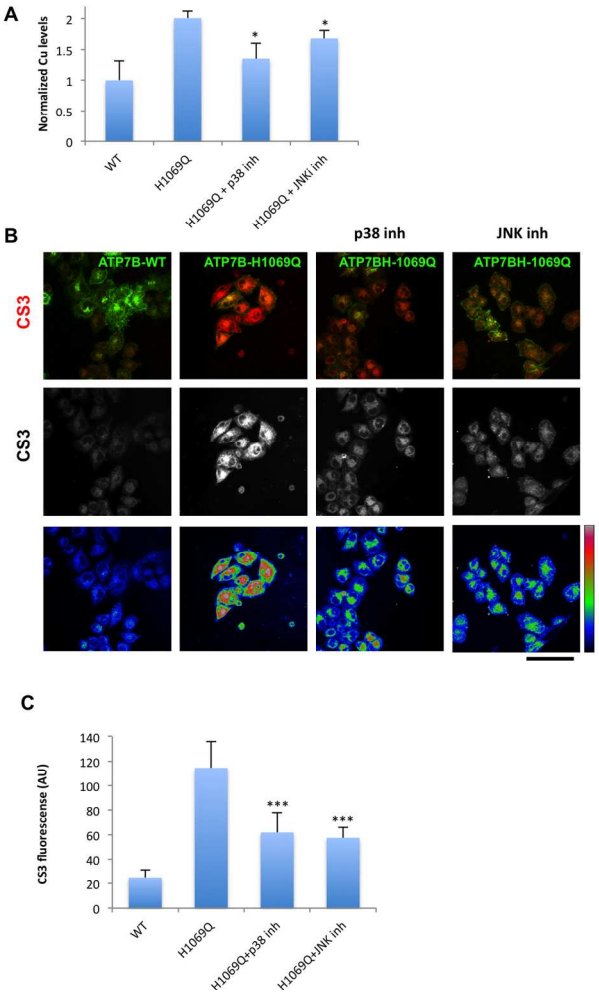

189x253mm (300 x 300 DPI)

Fig. 8. Chesi et al.

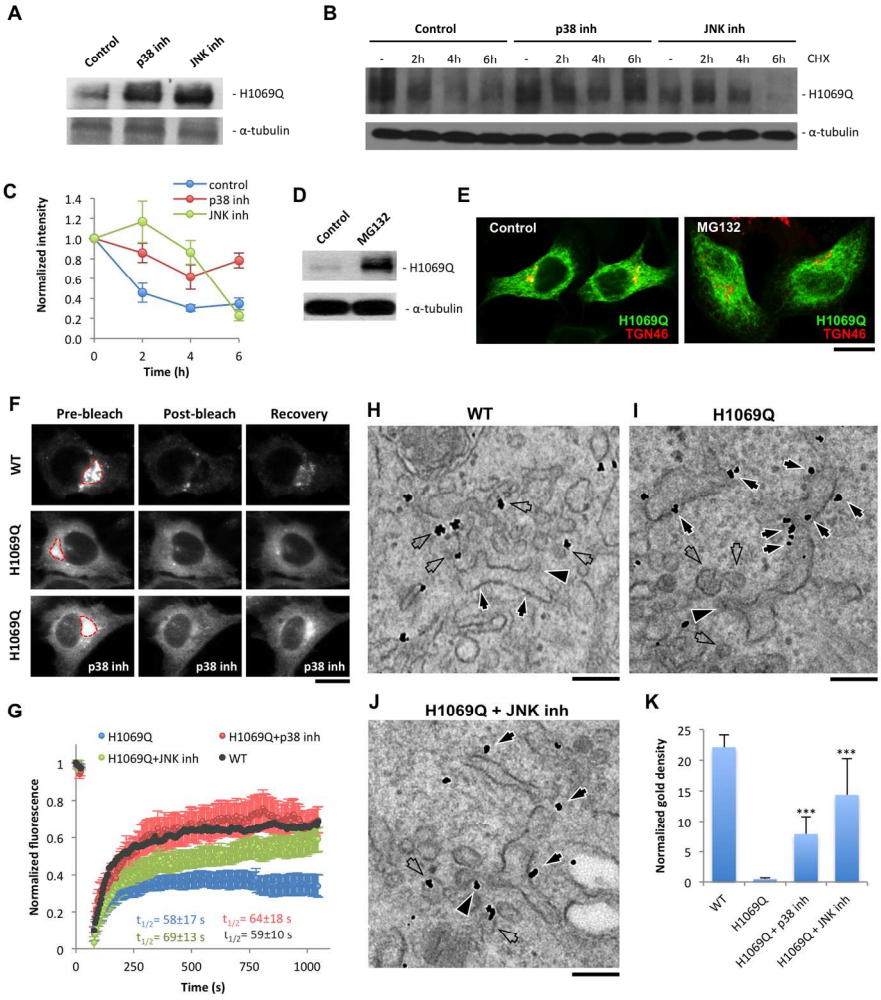

189x253mm (300 x 300 DPI)

SUPPLEMENTARY FIGURE LEGENDS

Sup. Fig. 1. ER retention of ATP7B^{H1069Q} mutant does not require activation of MEK/ERK signaling pathway.

(A) HepG2 cells were infected with Ad-ATP7B^{WT}-GFP or Ad-ATP7B^{H1069Q}-GFP and prepared western blot to reveal levels of phosphorylated and total ERK (p-ERK and ERK respectively). Both p-ERK and ERK levels did not exhibit significant changes in cells expressing ATP7B^{H1069Q} mutant. **(B)** HepG2 cells were infected withAd-ATP7B^{H1069Q}-GFP and incubated for 2h with BCS. Specific inhibitors of MEK/ERK, PD318088 (5μM) or GSK1120212 (5μM), were added to the cells 24h before fixation (as indicated in corresponding panels). Fixed cells were than labeled for TGN46 and visualized under confocal microscope. Treatment with each inhibitor did not recover ATP7B^{H1069Q} from the ER to the TGN. Scale bar: 5μm (B).

Sup. Fig. 2. Characterization of the impact of p38 and JNK inhibitors on trafficking of ATP7B and its mutant.

(A) Hela cells were infected with Ad-ATP7B^{WT}-GFP incubated overnight exposure to 200 μM BCS and fixed or incubated for additional 2h with 100 μM $CuSO_4$ (as indicated on panels). ATP7B^{WT} moves from the Golgi (arrowheads) to PM and vesicles (arrows) in response to $CuSO_4$. p38 inhibitor SB202190 (5μM) or JNK inhibitor SP600125 (2μM) were added to the cells 24h before fixation (as indicated in corresponding panels). Both inhibitors did not affect ability of ATP7B^{WT} to traffic from the Golgi to PM and vesicles (arrows in bottom row) in response to increased Cu. **(B)** Hela cells were infected with Ad-ATP7B^{H1069Q}-GFP fo 2h with 100 μM $CuSO_4$ (as indicated on panels). p38 inhibitor SB202190 or JNK inhibitor SP600125 were added to the cells 24h before fixation at different concentrations. Then the cells were stained for TGN46 and analyzed under confocal microscope. Percentage of the cells (average ± SD, n=10 fields) with ATP7B signal in the ER was calculated. Both p38 and JNK inhibitors reduced percentage of the

cells that exhibit ATP7B^{H1069Q} in the ER in concentration-dependent manner. Scale bar: 5 μm (A).

Sup. Fig. 3. p38 inhibitor, JNK inhibitor or their mixture correct ATP7B^{H1069Q} localization with similar strength.

(A) HeLa cells were infected with Ad-ATP7B^{WT}-GFP or Ad-ATP7B^{H1069Q}-GFP, incubated for 2h with 200 μM BCS and fixed. p38 inhibitor SB202190 (5μM) or JNK inhibitor SP600125 (2μM) or mixture of both inhibitors were added to the cells 24h before fixation (as indicated in corresponding panels). Fixed cells were than labeled for TGN46 and visualized under confocal microscope. p38 and JNK inhibitors as well as their mixture corrected ATP7B^{H1069Q} from the ER to the Golgi with similar amplitude. **(B)** Fluorescence of ATP7B signal in the Golgi (average ± SD, n=40 cells) was quantified and normalized to total cell fluorescence. p38 and JNK inhibitors (or their mixture) caused increase of ATP7B^{H1069Q} signal in the Golgi region. Exposure of the cells to the mixture of inhibitors does not significantly increase ATP7B^{H1069Q} signal in the Golgi when compared to each inhibitor alone. **(C)** The percentage of the cells (average ± SD, n=10 fields) with an ATP7B signal in the ER, or Golgi was calculated. p38 and JNK inhibitors alone as well as their combination reduced the percentage of the cells exhibiting ATP7B^{H1069Q} in the ER and increases the number of cells in which the mutant was corrected to the Golgi. Single inhibitors and their mixture exhibit similar strength in correction of ATP7B^{H1069Q} intracellular phenotype. ✻✻✻- $p<0.001$; ✻✻- $p<0.01$; ✻- $p<0.05$; ns – $p>0.05$ (t-test). Scale bar: 5 μm (A).

Sup. Fig. 4. Acute treatment with p38 or JNK inhibitor does not rescue ATP7B^{H1069Q} mutant from the ER.

(A) HeLa cells were infected with Ad-ATP7B^{H1069Q}-GFP and incubated for 2h with 100 μM $CuSO_4$. p38 inhibitor or JNK inhibitor were added to the cells 1h before fixation (as indicated in corresponding panels). Fixed cells were than labeled for TGN46 and visualized under confocal microscope. Short-term treatment with either p38 orJNK inhibitor did not recover ATP7B^{H1069Q} from the ER. **(B)** Percentage of the cells (average ± SD, n=10 fields) with ATP7B signal in the ER, was calculated. Both p38 and JNK

inhibitors did not reduce percentage of the cells that exhibit ATP7B^{H1069Q} in the ER after 1h treatment. Scale bar: 5 μm (A).

Sup. Fig. 5. p38 and JNK inhibitors increase ATP7B^{H1069Q} amounts in plasma membrane subcellular fraction.

(A) HepG2 cells were infected with Ad-ATP7B^{WT}-GFP and incubated for 2h with 100 μM $CuSO_4$. The cells were then subjected to subcellular fractionation (see Methods) and isolated membrane fractions labeled with different markers. Western blot indicates that ATP7B^{WT} was enriched in fractions #5 and #10. However, fractions #2-5 were cross-contaminated with ER (PDI), Golgi (GM130) and at some extent with plasma membrane (Na/K-ATPase) indicating poor separation between corresponding organelles. In contrast, fraction #10 contained only Na/K-ATPase demonstrating significant enrichment in plasma membranes (PMs). Therefore, Na/K-ATPase positive PM fractions were used further for evaluation of ATP7B^{WT} or ATP7B^{H1069Q} delivery to the cell surface. **(B)** HepG2 cells were infected with Ad-ATP7B^{WT}-GFP or Ad-ATP7B^{H1069Q}-GFP and treated with $CuSO_4$ and subjected to fractionation as in panel A. p38 inhibitor or JNK inhibitor were added to the cells 24h before fractionation procedure. Light PM fractions (#10-12) were prepared for Western blot and labeled with antibodies against GFP and against Na/K-ATPase. Na/K-ATPase-positive PM fractions from the p38 inhibitor- or JNK inhibitor-treated cells exhibit higher amounts of ATP7B^{H1069Q} then the same fractions from untreated cells indicating that both inhibitors facilitate ATP7B^{H1069Q} delivery to the cell surface. **(C)** ATP7B signal in fractions #10 (shown in panel B) was quantified using ImageJ software and normalized for Na/K-ATPase signal in corresponding lanes. Plot shows that both p38 and JNK inhibitors increase quantities of ATP7B^{H1069Q} associated with PM fractions.

Sup. Fig. 6. Suppression of p38 and JNK allows ATP7B^{H1069Q} to reach canalicular surface of polarized HepG2 cells.

HepG2 cells were grown at the conditions that allow their full polarization (see Methods). Then the cells were infected with Ad-ATP7B^{WT}-GFP (A) or Ad-ATP7B^{H1069Q}-GFP (B-D) and incubated for 4h with 100 μM $CuSO_4$. p38 (C) or JNK (D) inhibitors were added

to the cells 24h before fixation. Fixed cells were labeled for canalicular marker MRP2 and visualized under confocal microscope. Cu induces delivery of $ATP7B^{WT}$ to the canalicular domain (A, arrows) while the mutant remains retained within the ER and does not reach the canalicular srface (B, arrows). Both p38 and JNK inhibitors allows $ATP7B^{H1069Q}$ to de delivered to the canalicular domain (C, D; arrows) in polarized HepG2 cells. Scale bar: 4 μm (A-D).

Sup. Fig. 7. Inhibitors of p38 and JNK reduce copper levels in cells expressing $ATP7B^{H1069Q}$ mutant.

HepG2 cells were infected with Ad-$ATP7B^{WT}$-GFP (A) or Ad-$ATP7B^{H1069Q}$-GFP (B-D), incubated for 2h with 100 μM $CuSO_4$ and loaded with CS3 before fixation. p38 (C) or JNK (D) inhibitors was added to the cells 24h before fixation. **(A, B)** Cells expressing $ATP7B^{H1069Q}$ exhibit higher CS3 signal (and hence Cu levels) than cells expressing $ATP7B^{WT}$. Arrows in B indicate $ATP7B^{H1069Q}$ –negative cells, which display CS3 levels similar to those detected in the neighbor cell expressing the mutant. This indicates that expression of mutant does not allow cells to efflux Cu efficiently. **(C, D)** Both p38 and JNK inhibitors decrease CS3 fluorescence in $ATP7B^{H1069Q}$-expressing cells. Arrows in C and D show higher CS3 levels in cells expressing lower $ATP7B^{H1069Q}$ amounts, indicating that capacity of p38/JNK-inhibitor treated cells to eliminate Cu correlates to amount of the expressed mutant. Scale bar: 10 μm (A-D).

Sup. Fig. 8. Inhibitors of p38 and JNK do not impact trafficking of VSVG.

(A) HeLa cells were transfected with DNA encoding temperature-sensitive version of VSVG-GFP, incubated overnight at 40°C to block the newly-synthetized protein in the ER and fixed directly (left column) or incubated at 32°C for additional time periods (to activate VSVG-GFP trafficking) as indicated in panels. p38 inhibitor (mid row) or JNK inhibitor (bottom row) were added to the cells 24h before fixation. Fixed cells were than analyzed using confocal microscopy. Both p38 and JNK inhibitors did not affect VSVG delivery from the ER to the Golgi (arrowheads) and further to the PM (arrows). **(B)** Percentage of the cells (average ± SD, n=10 fields) with ATP7B signal in the ER, Golgi or PM was calculated. Cells exhibit similar dynamics of VSVG progression through the

secretory pathway in control cells and in cells treated with p38 or JNK inhibitor. Scale bar: 5.2 μm (A).

Sup. Fig. 9. p38 and JNK inhibitors does not affect interaction of ATP7B^{H1069Q} with COMMD1.

(A) HepG2 cells expressing COMMD1-GST were infected with Ad-ATP7B^{WT}-GFP or Ad-ATP7B^{H1069Q}-GFP, incubated for 2h with 100 μM $CuSO_4$ and lysed. ATP7B^{WT} and ATP7B^{H1069Q} we pulled down from lysates using anti-GFP antibody. Both immuno-precipitates (IPs) and total cell lysates were subjected to Western blot to reveal ATP7B and COMMD1. Western blot shows higher levels of COMMD1 in ATP7B^{H1069Q} IP, indicating enhanced interaction of the mutant with COMMD1. **(B)** HepG2 cells expressing COMMD1-GST were infected with Ad-ATP7B^{H1069Q}-GFP, treated with Cu and prepared for IP and Western blot as described in panel A. p38 or JNK inhibitor was added to the cells 24h before they were lysed. Neither inhibitor reduced COMMD1 binding to ATP7B^{H1069Q}, indicating that this interaction is unlikely to be involved in mutant correction by p38 or JNK inhibitors.

Fig. S1. Chesi et al.

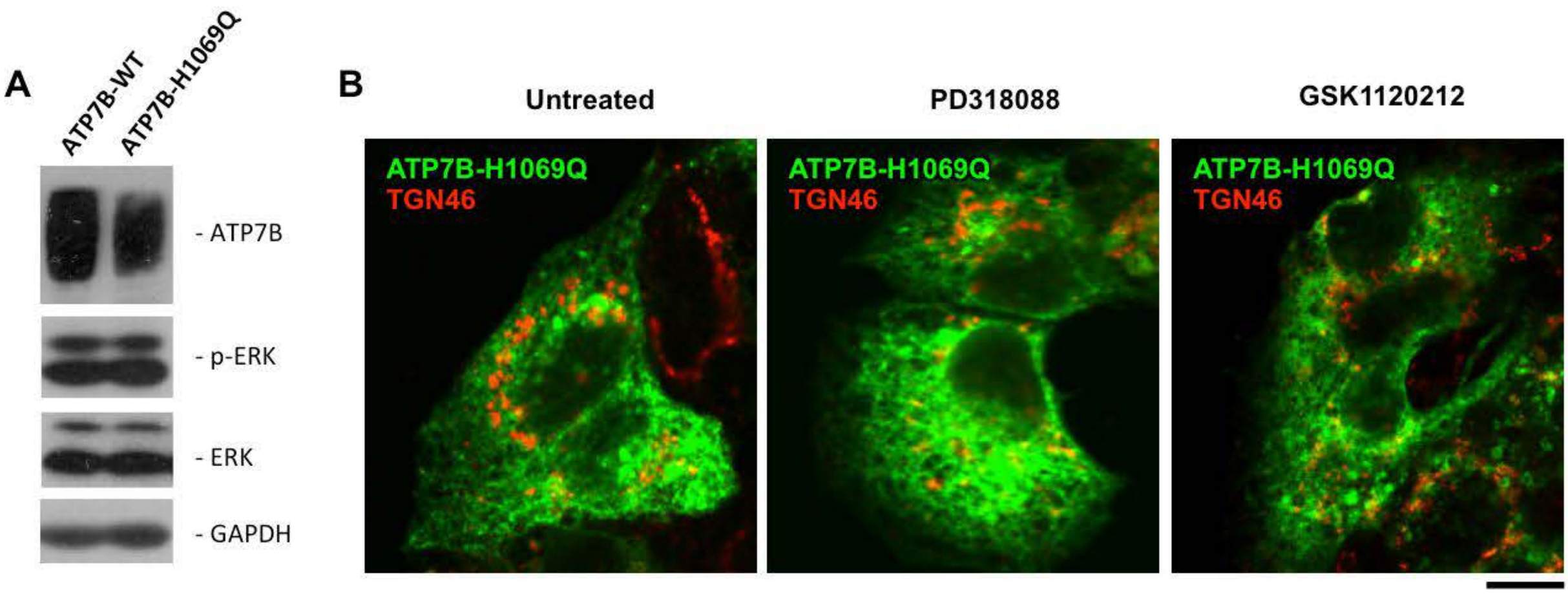

Fig. S2. Chesi et al.

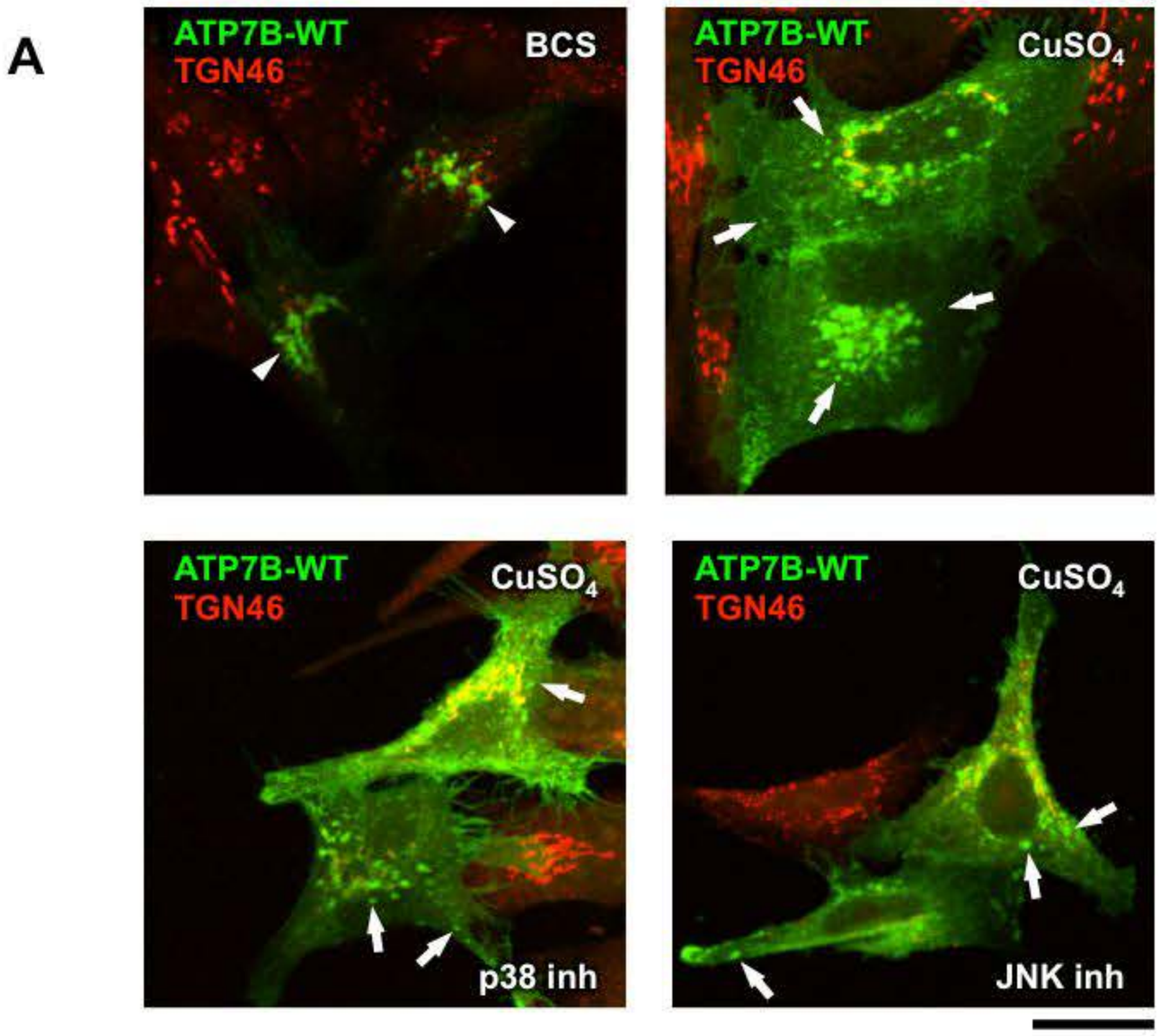

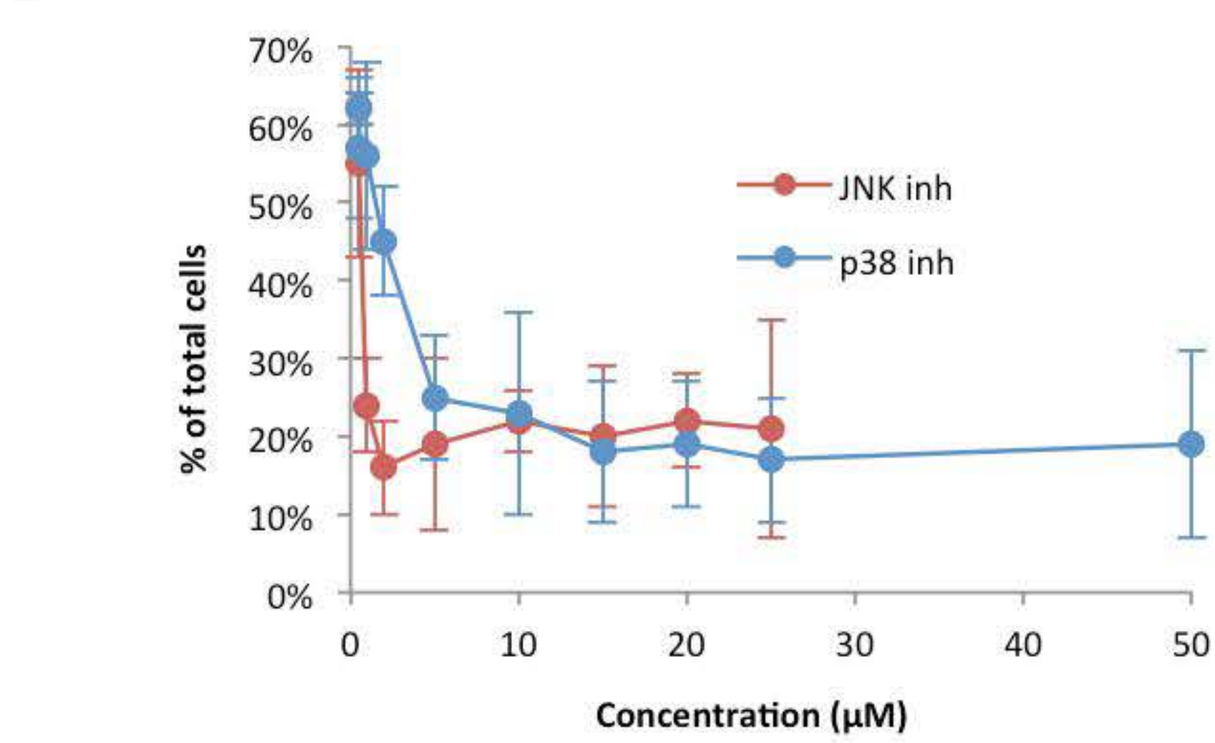

Fig. S3. Chesi et al.

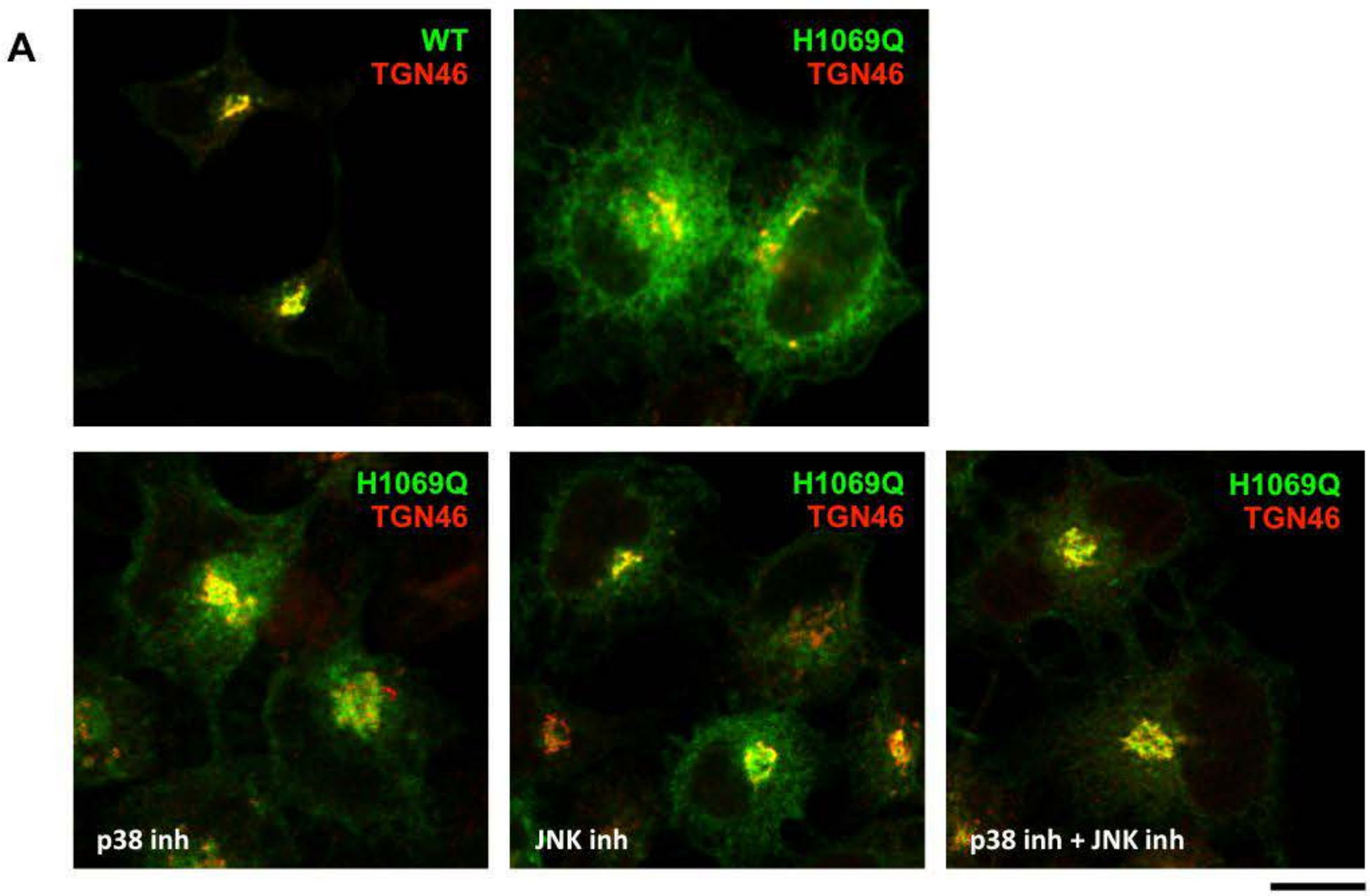

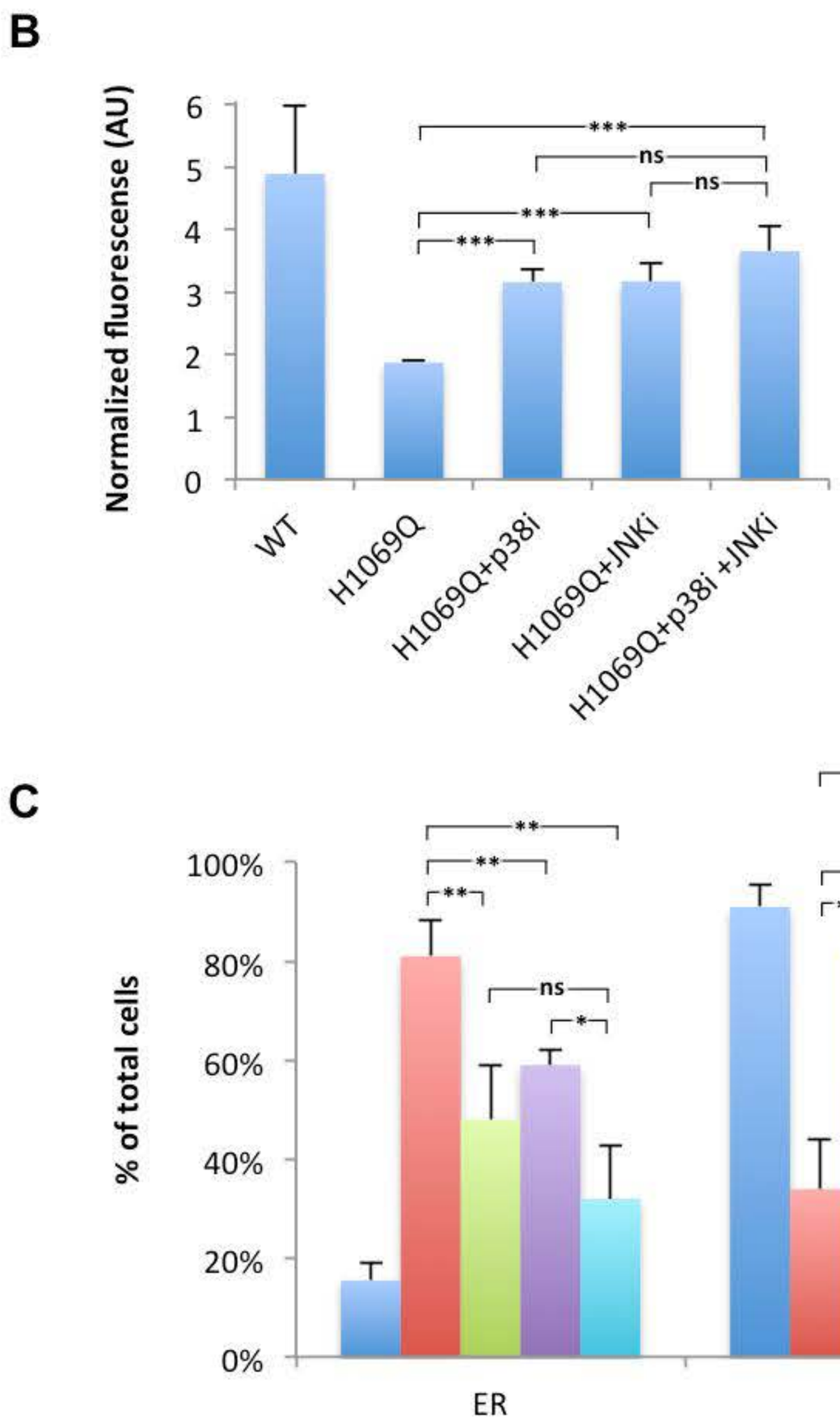

Fig. S4. Chesi et al.

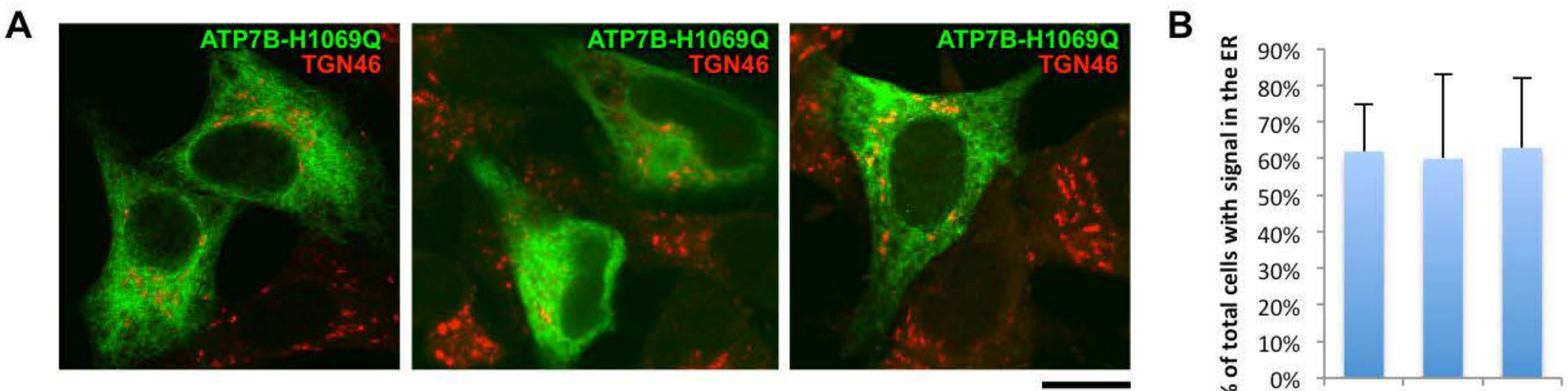

Fig. S5. Chesi et al.

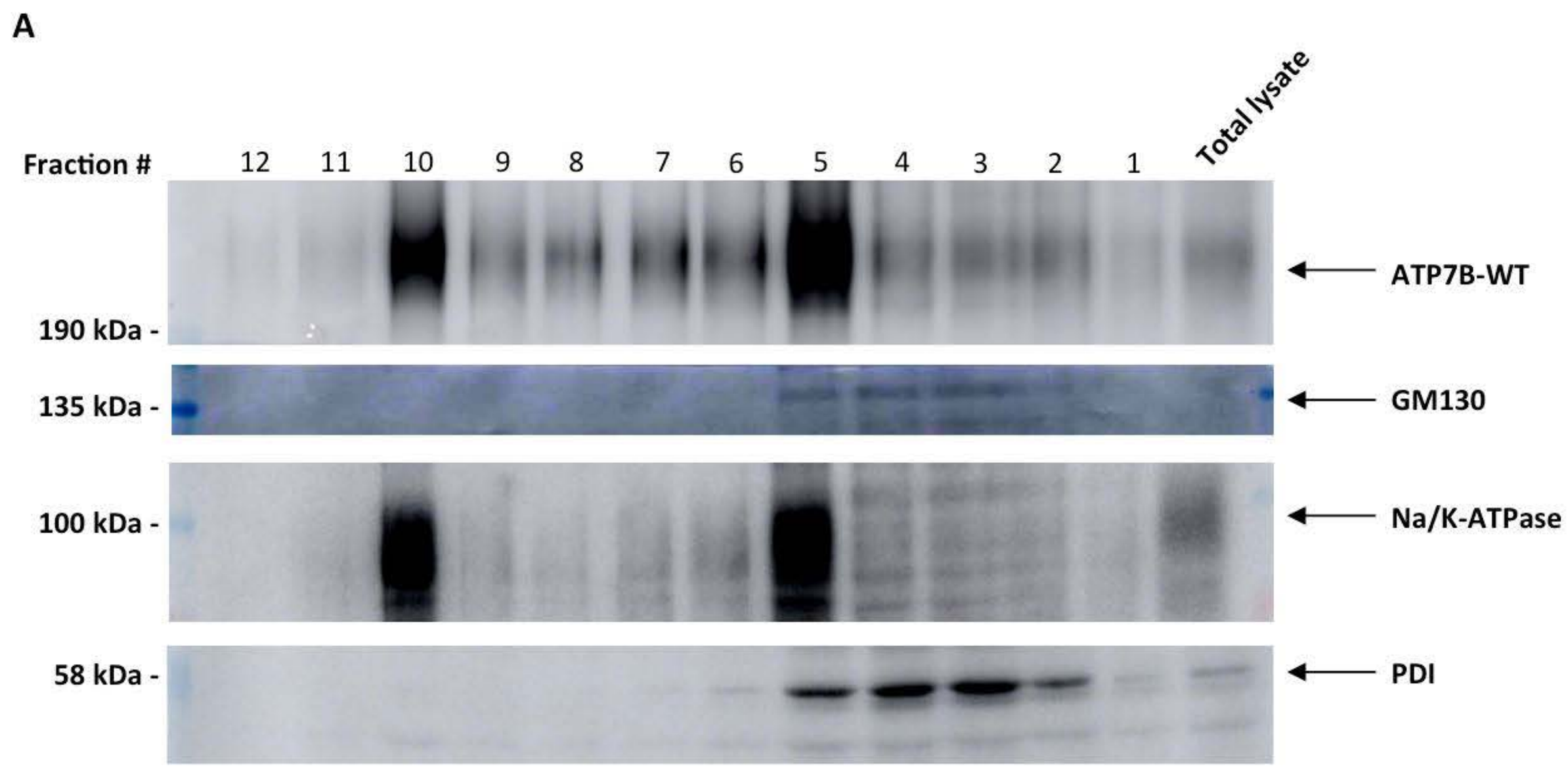

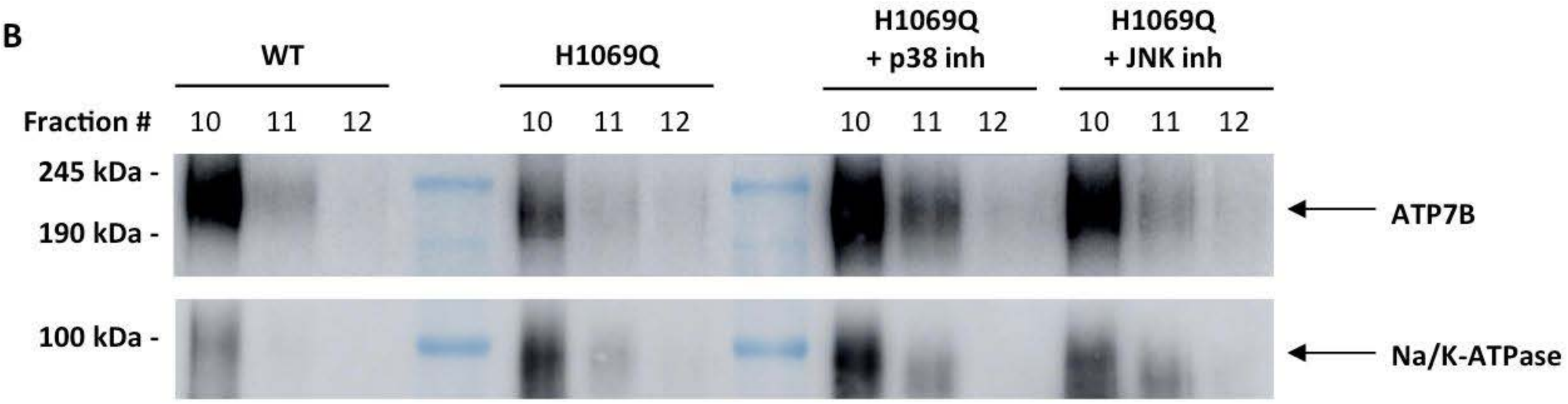

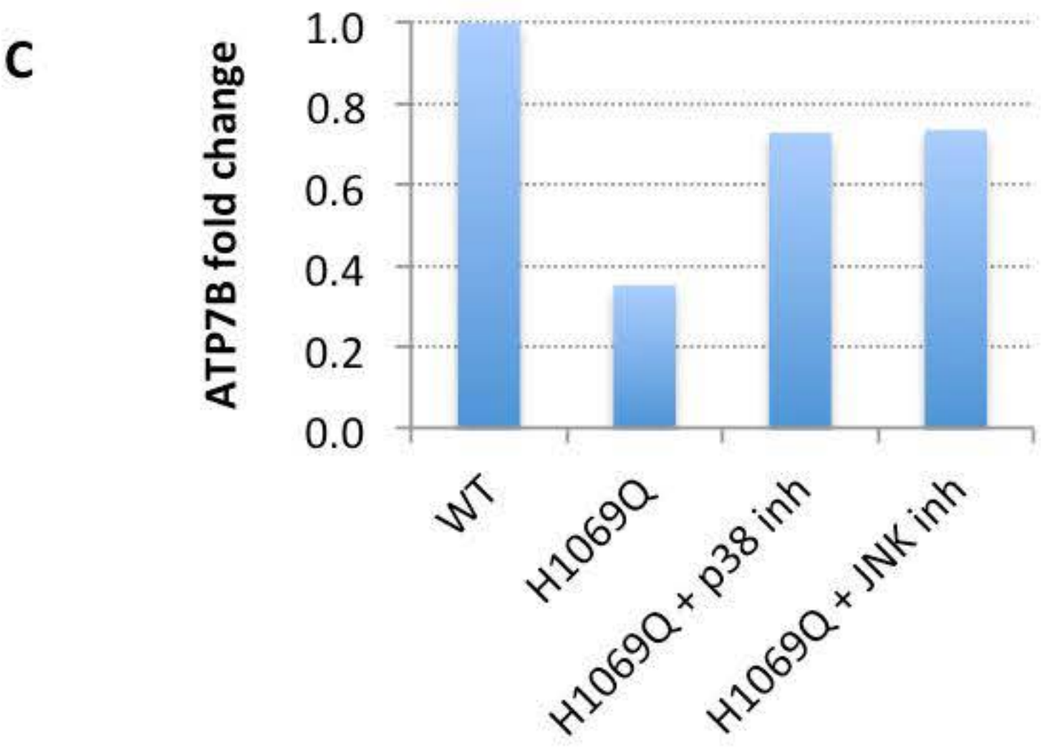

Fig. S6. Chesi et al.

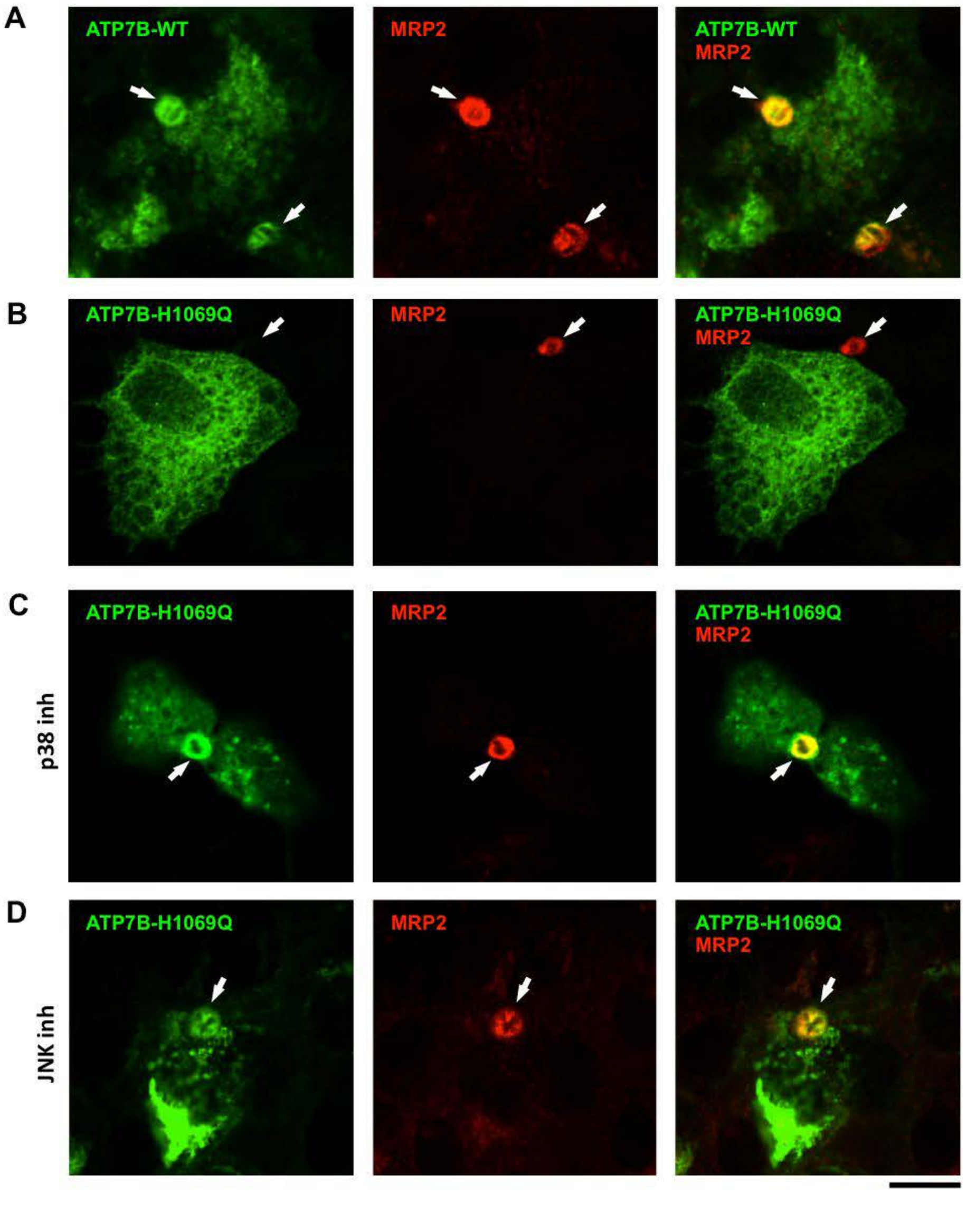

Fig. S7. Chesi et al.

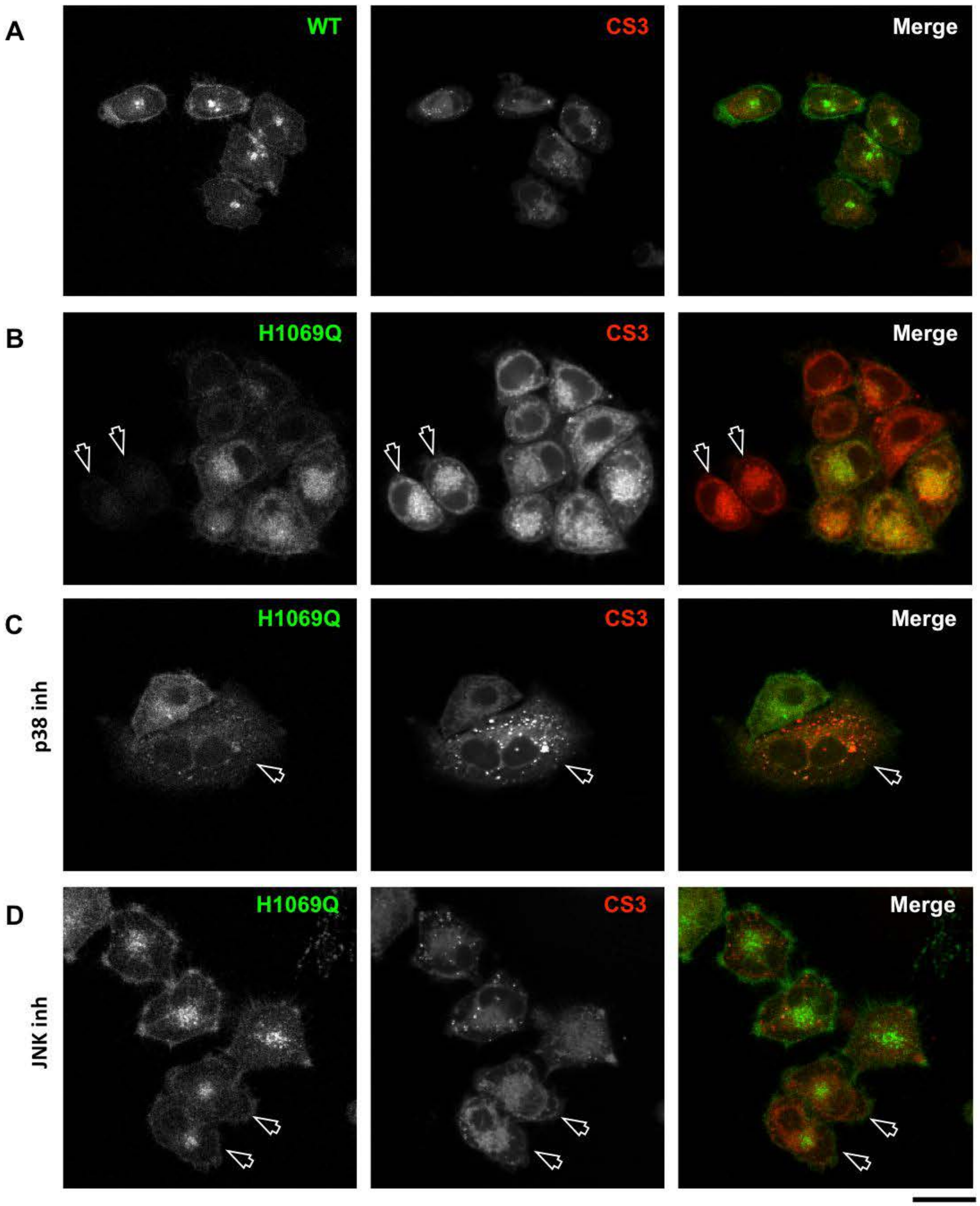

Fig. S8. Chesi et al.

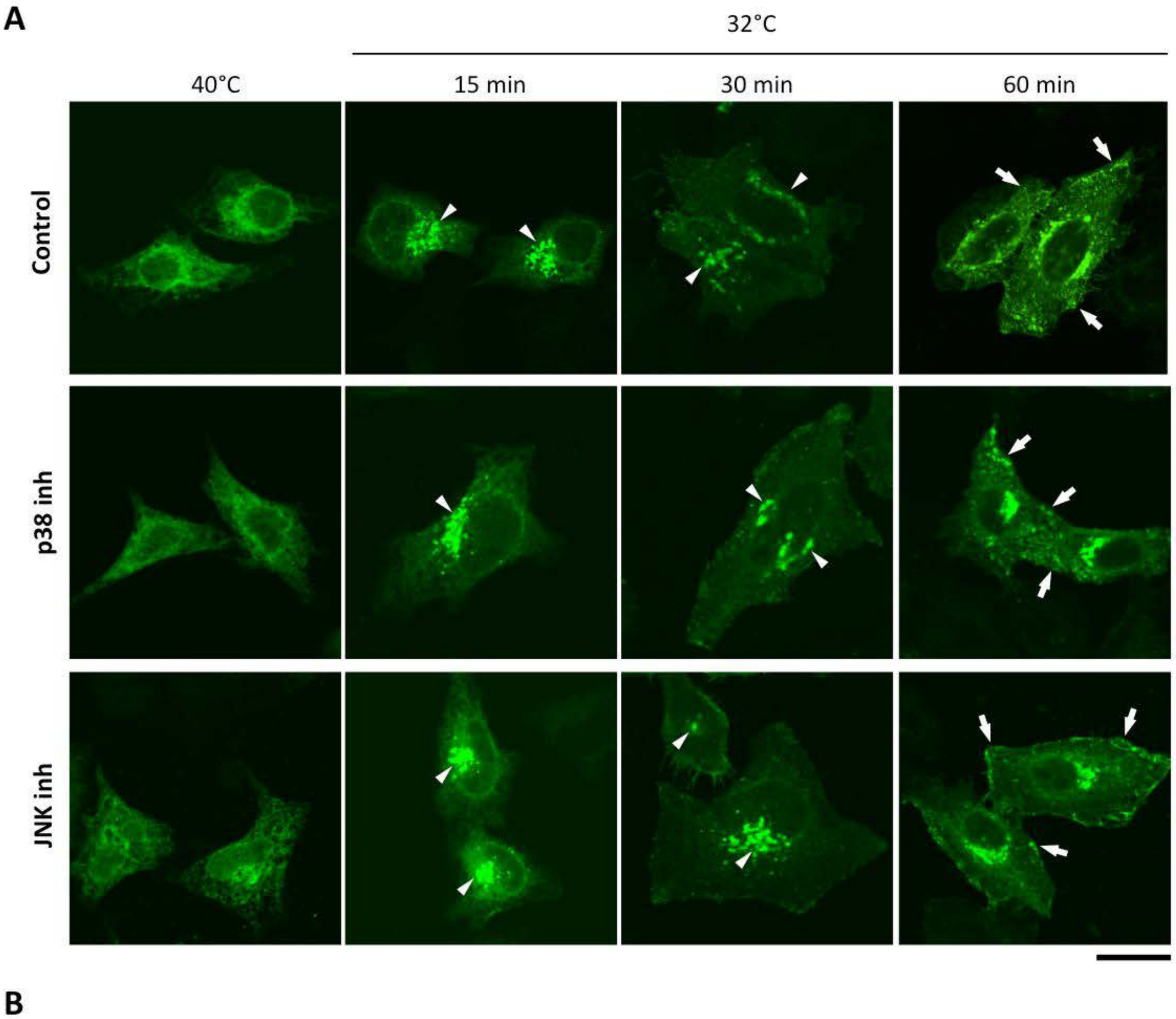

SUPPLEMENTARY TABLE 1.
Gene ontology (GO) categories of genes differentially expressed in ATP7B-H1069Q expressing cells versus ATP7B-WT expressing cells.

Gene Ontology (GO) Categories	Gene Ontology (GO) ID	Number of differentially expressed Genes with this GO category	Name of differentially expressed Genes with this GO category	Population Hits (PH)	Population Total (PT)	Fold Enrichment (FE)	False Discovery Rate (FDR)
regulation of apoptosis	GO:0042981	41	CADM1, MCL1, CLU, TAF9B, SOX4, CDH1, CHEK2, SFN, PTEN, MAGED1, TDGF3, NOD2, TP53I3, CDKN2A, SQSTM1, CDKN2C, CDKN2D, AGT, TDGF1, PYCARD, FAIM, CAT, FAS, FOSL1, HELLS, MAP2K6, KNG1, TXNIP, DEPDC6, MSH6, LGALS1, ITGA1, SKP2, BIRC3, CDK5, SOD2, BNIP3L, AVEN, ID3, TNFAIP3, IGFBP3, IFI6	804	13528	2,41210034	5,78E-04
regulation of cell proliferation	GO:0042127	35	FGFR2, BLM, IFITM1, IL18, CLU, IFI30, SOX4, SFN, PTEN, TIMP1, TRIB1, MAGED1, CD47, WARS, TDGF3, CD9, CDKN2A, CDKN2C, CDKN2D, AGT, TDGF1, SERPINE1, FOSL1, TXNIP, STS, TESC, IL8, EGR4, SPARC, CDKN3, SOD2, CORO1A, CBLB, EREG, BTG3, IGFBP3	787	13528	2,10358891	0,092770639
response to drug	GO:0042493	15	TXNIP, NAT8B, NAT8, MFSD9, MAT2A, CDH1, PTEN, SOD2, SERPINA7, CA9, ENO3, GNAS, LOX, FOSL1, PDZK1, MAP2K6	216	13528	3,28477078	0,341239702
regulation of cell cycle	GO:0051726	19	BLM, NEK2, SKP2, NUSAP1, ANAPC10, CHEK2, SFN, OBFC2A, CDKN3, CDK5, PTEN, CDT1, CDKN2A, EREG, CDKN2C, CDKN2D, BTG3, ID3, FOSL1	331	13528	2,71514588	0,404894167
regulation of cellular component size	GO:0032535	16	FGFR2, DEPDC6, TAF9B, SFN, CSRP2, N6AMT1, LEFTY1, CORO1A, CDKN2A, NDRG4, CDKN2C, MAPT, CDKN2D, AGT, TMSB4X, TMSL3	271	13528	2,79266121	1,099341419
oxidation reduction	GO:0055114	27	CYP24A1, SORD, PYROXD1, IFI30, GLDC, GPX2, TP53I3, P4HA2, P4HA1, PLOD2, IDH2, HSD17B6, BDH2, LOX, CAT, HADH, GPD1, NOX3, MTHFD2L, SOD2, OGFOD1, G6PD, BLVRB, PCYOX1, DIO1, GLYR1, AOC3	639	13528	1,9986211	1,758146094
positive regulation of immune system process	GO:0002684	14	MICB, BLM, CADM1, IL18, F2RL1, CLU, AQP3, CD47, CBLB, NOD2, CORO1A, EREG, SPG21, CFD	238	13528	2,78239408	2,783907866
DNA replication	GO:0006260	12	POLD3, PRIM1, GINS2, RFC4, BLM, POLE2, DTL, MRE11A, CDKN2D, MCM10, CHAF1A, CDT1	190	13528	2,98741259	3,954136316
response to DNA damage stimulus	GO:0006974	18	EXO1, MSH6, NUDT1, BLM, DTL, MRE11A, SFN, CHEK2, OBFC2A, ATMIN, SOD2, POLD3, RFC4, POLE2, FANCI, CDKN2D, CHAF1A, MAP2K6	373	13528	2,28260747	4,081799187
regulation of cell adhesion	GO:0030155	10	KNG1, CD47, TDGF3, TESC, CDKN2A, IL8, IL18, TDGF1, SERPINI1, PTEN, DPP4	137	13528	3,45260579	4,180275525

Gene ontology descriptions of biological processes were assigned on the basis of the informations retrieved from DAVID (http://david.abcc.ncifcrf.gov/), considering a False Discovery Rate (FDR) less than 5; Population Hits (PH) corresponds to the number of genes of each GO category on the whole background list; Population Total (PT) corresponds to the total number of genes on the whole background list; Fold Enrichment (FE) estimates the enrichment degree of the corresponding GO category

SUPPLEMENTARY TABLE 2. List of ATP7B-WT-specific interactors.

Protein	CODE SP	GENE NAME	# Peptides	MW [kDa]	
Transferrin receptor protein 1	**P02786**	**TFRC**	**4**	**85**	
Peptide Sequences	Modifications	IonScore	Charge	MH+ [Da]	ΔM [ppm]
LAVDEEENADNNTK		53	2	1561.73	22.5
LLNENSYVPR		18	2	1204.81	250
SSGLPNIPVQTISR		28	2	1468.97	96
VEYHFLSPYVSPK		15	3	1566.08	183
Guanine nucleotide-binding protein subunit beta-2-like 1	**P63244**	**GNB2L1**	**11**	**35**	
Peptide Sequences	Modifications	IonScore	Charge	MH+ [Da]	ΔM [ppm]
IIVDELKQEVISTSSK		79	2	1789.27	155
VWQVTIGTR		47	2	1059.69	92.7
LWDLTTGTTTR		46	2	1264.85	158
YWLCAATGPSIK		46	2	1366.93	183
LWDLTTGTTTRR		36	3	1421.03	198
DETNYGIPQR		36	2	1192.63	61.6
LTRDETNYGIPQR		33	3	1562.96	111
VWNLANCK		32	2	1004.63	134
FSPNSSNPIIVSCGWDK		45	2	1907.94	29.9
IWDLEGK		26	2	860.61	188
60S ribosomal protein L7	**P18124**	**RPL7**	**8**	**29**	
Peptide Sequences	Modifications	IonScore	Charge	MH+ [Da]	ΔM [ppm]
IVEPYIAWGYPNLK		81	2	1663.17	123
IALTDNALIAR		71	2	1170.81	195
SVNELIYKR		38	2	1121.69	54.8
ASINMLR		35	2	804.51	91
EVPAVPETLK		34	2	1082.65	40.3
QIFNGTFVK		33	2	1053.77	190
SVNELIYK		32	2	965.63	106
AGNFYVPAEPK		30	2	1192.75	128
ADP/ATP translocase 3	**P12236**	**SLC25A6**	**7**	**33**	
Peptide Sequences	Modifications	IonScore	Charge	MH+ [Da]	ΔM [ppm]
DFLAGGIAAAISK		99	2	1233.89	170
YFPTQALNFAFK		54	2	1446.97	160
LLLQVQHASK		39	2	1136.79	100
GNLANVIR		38	2	856.53	38.4
GAWSNVLR		35	2	902.61	75.9
AAYFGVYDTAK		32	2	1205.73	124
EQGVLSFWR		26	2	1121.81	178
Vesicle-associated membrane protein-associated protein B/C	**O95292**	**VAPB**	**3**	**27**	
Peptide Sequences	Modifications	IonScore	Charge	MH+ [Da]	ΔM [ppm]
GPFTDVVTTNLK		66	2	1291.81	95.7
TVQSNSPISALAPTGK		51	2	1570.79	5.87
FRGPFTDVVTTNLK		15	3	1595.24	243
Glutathione S-transferase omega-1	**P78417**	**GSTO1**	**6**	**27**	
Peptide Sequences	Modifications	IonScore	Charge	MH+ [Da]	ΔM [ppm]
VPSLVGSFIR		51	2	1074.73	151
HEVININLK		46	2	1079.71	85.3
GSAPPGPVPEGSIR		32	2	1320.79	77.4
LLPDDPYEK		31	2	1089.65	135
FCPFAER		17	2	925.56	166
EFTKLEEVLTNK		17	3	1450.88	73.6
Ribonucleoside-diphosphate reductase subunit M2	**P31350**	**RRM2**	**2**	**51**	
Peptide Sequences	Modifications	IonScore	Charge	MH+ [Da]	ΔM [ppm]
FSQEVQITEAR		67	2	1307.61	-35.41
IEQEFLTEALPVK		58	2	1516.95	83.8
14-3-3 protein eta	**Q04917**	**YWHAH**	**2**	**28**	
Peptide Sequences	Modifications	IonScore	Charge	MH+ [Da]	ΔM [ppm]
AVTELNEPLSNEDR		82	2	1586.85	54.9
NSVVEASEAAYK		58	2	1267.65	28.6
LIM domain only protein 7	**Q8WWI1**	**LMO7**	**4**	**158**	
Peptide Sequences	Modifications	IonScore	Charge	MH+ [Da]	ΔM [ppm]
TSTTGVATTQSPTPR		74	2	1504.79	21.6
ISINQTPGK		45	2	957.61	79.8
WIDATSGIYNSEK		38	2	1484.33	422
RGESLDNLDSPR		35	3	1358.96	221
ATP-dependent Clp protease ATP-binding subunit clpX-like, mit	**O76031**	**CLPX**	**5**	**58**	
Peptide Sequences	Modifications	IonScore	Charge	MH+ [Da]	ΔM [ppm]
DVGGEGVQQGLLK		68	2	1299.67	-13.55
LLEGTIVNVPEK		47	2	1312.03	214
LLQDANYNVEK		32	2	1306.89	175

SIIKEPESAAEAVK		28	3	1472.33	364
TLLAQTLAK		28	2	958.75	167
Eukaryotic translation initiation factor 4 gamma 2	**P78344**	**EIF4G2**	**2**	**102**	
Peptide Sequences	Modifications	IonScore	Charge	MH+ [Da]	ΔM [ppm]
TQTPPLGQTPQLGLK		68	2	1578.97	55.6
SYLAQFAAR		59	2	1026.67	133
Estradiol 17-beta-dehydrogenase 8	**Q92506**	**HSD17B8**	**2**	**27**	
Peptide Sequences	Modifications	IonScore	Charge	MH+ [Da]	ΔM [ppm]
SALALVTGAGSGIGR		91	2	1329.87	93.3
AGVIGLTQTAAR		55	2	1157.69	25
signal recognition particle receptor subunit beta	**Q9Y5M8**	**SRPRB**	**5**	**30**	
Peptide Sequences	Modifications	IonScore	Charge	MH+ [Da]	ΔM [ppm]
SAAPSTLDSSSTAPAQLGK		77	2	1788.97	42.1
GDVGSADIQDLEK		63	2	1346.81	126
VADGGGAGGTFQPYLDTLR		53	2	1894.98	33.4
SAAPSTLDSSSTAPAQLGKK		24	3	1916.99	1.62
LQFLER		22	2	805.55	119
Cell cycle and apoptosis regulator protein 2	**Q8N163**	**DBC1**	**6**	**103**	
Peptide Sequences	Modifications	IonScore	Charge	MH+ [Da]	ΔM [ppm]
TLAAEMQELR		56	2	1161.67	68.5
VQTLSNQPLLK		45	2	1240.87	118
FSATEVTNK		34	2	996.65	154
LTPLQLEIQR		28	2	1210.89	147
SPAPPLLHVAALGQK		27	3	1499.03	108
IQVSSEKEAAPDAGAEPITADSDPAYSSK		25	3	2934.28	-30.54
ATP synthase subunit gamma, mitochondrial	**P36542**	**ATP5C1**	**3**	**33**	
Peptide Sequences	Modifications	IonScore	Charge	MH+ [Da]	ΔM [ppm]
IYGLGSLALYEK		51	2	1326.91	138
SEVATLTAAGK		44	2	1047.73	157
HLLIGVSSDR		41	2	1096.61	1.64
Large proline-rich protein BAG6	**P46379**	**BAG6**	**3**	**114**	
Peptide Sequences	Modifications	IonScore	Charge	MH+ [Da]	ΔM [ppm]
AGSSESIAAFIQR		64	2	1336.85	110
LINLVGESLR		36	2	1113.89	207
LQEDPNYSPQRFPNAQR		24	3	2060.17	92.8
Ubiquitin-associated protein 2	**Q5T6F2**	**UBAP2**	**3**	**117**	
Peptide Sequences	Modifications	IonScore	Charge	MH+ [Da]	ΔM [ppm]
DGSLANNPYPGDVTK		63	2	1547.79	38.2
SQPEPSPVLSQLSQR		32	2	1652.93	43.9
AAPLVTSGK		28	2	843.53	46.6
Ran-specific GTPase-activating protein	**P43487**	**RANBP1**	**2**	**23**	
Peptide Sequences	Modifications	IonScore	Charge	MH+ [Da]	ΔM [ppm]
TLEEDEEELFK		55	2	1381.89	185
FASENDLPEWKER		44	3	1621.01	154
Cation-independent mannose-6-phosphate receptor	**P11717**	**IGF2R**	**2**	**266**	
Peptide Sequences	Modifications	IonScore	Charge	MH+ [Da]	ΔM [ppm]
VPIDGPPIDIGR		48	2	1248.91	175
YDLSALVR		37	2	936.75	254
B-cell receptor-associated protein 31	**P51572**	**BCAP31**	**2**	**28**	
Peptide Sequences	Modifications	IonScore	Charge	MH+ [Da]	ΔM [ppm]
LDVGNAEVKLEEENR		59	3	1715.09	137
AENQVLAMR		51	2	1031.67	138
NADH dehydrogenase [ubiquinone] 1 alpha subcomplex subunit 2	**O43678**	**NDUFA2**	**2**	**11**	
Peptide Sequences	Modifications	IonScore	Charge	MH+ [Da]	ΔM [ppm]
ALENVLSGKA		45	2	1001.64	90.1
YAFGQETNVPLNNFSADQVTR		55	3	2371.25	52.4
Inositol-3-phosphate synthase 1	**Q9NPH2**	**ISYNA1**	**3**	**61**	
Peptide Sequences	Modifications	IonScore	Charge	MH+ [Da]	ΔM [ppm]
VGPVAATYPMLNK		50	2	1360.93	150
ADNLIPGSR		27	2	942.71	226
VFVGGDDFK		21	2	983.69	213
EH domain-containing protein 1	**Q9H4M9**	**EHD1**	**3**	**61**	
Peptide Sequences	Modifications	IonScore	Charge	MH+ [Da]	ΔM [ppm]
LLDTVDDmLANDIAR	M8(Oxidation)	61	2	1691.01	107
HLIEQDFPGMR		18	2	1343.29	474
KLNAFGNAFLNR		10	3	1364.51	-167.09
5'-3' exoribonuclease 2	**Q9H0D6**	**XRN2**	**3**	**109**	
Peptide Sequences	Modifications	IonScore	Charge	MH+ [Da]	ΔM [ppm]
NSLGGDVLFVGK		53	2	1205.88	199
GVGAEPLLPWNR		18	2	1308.9	158
AALEEVYPDLTPEETRR		50	3	1989.17	92.1
60S acidic ribosomal protein P1	**P05386**	**RPLP1**	**2**	**12**	
Peptide Sequences	Modifications	IonScore	Charge	MH+ [Da]	ΔM [ppm]

KEESEESDDDMGFGLFD		62	2	1949.9	78.7
AAGVNVEPFWPGLFAK		55	2	1703.03	80.8
NADH dehydrogenase [ubiquinone] 1 beta subcomplex subunit 4	**O95168**	**NDUFB4**	**3**	**15**	
Peptide Sequences	Modifications	IonScore	Charge	MH+ [Da]	ΔM [ppm]
TLPETLDPAEYNISPETR		56	2	2045.96	-14.59
GLIENPALLR		53	2	1095.73	73.7
TINVYPNFRPTPK		20	2	1547.57	476
Conserved oligomeric Golgi complex subunit 5	**Q9UP83**	**COG5,**	**2**	**91**	
Peptide Sequences	Modifications	IonScore	Charge	MH+ [Da]	ΔM [ppm]
NPPSSDELDGIIK		47	2	1384.67	-16.41
STMPTPGNTAALR		19	2	1316.95	220
Protein transport protein Sec24C	**P53992**	**SEC24C**	**3**	**118**	
Peptide Sequences	Modifications	IonScore	Charge	MH+ [Da]	ΔM [ppm]
SPVESTTEPPAVR		45	2	1369.77	56.2
GTEPFVTGVR		22	2	1062.69	127
YASFQVENDQER		11	2	1485.77	75.6
14-3-3 protein theta	**P27348**	**YWHAQ**	**2**	**28**	
Peptide Sequences	Modifications	IonScore	Charge	MH+ [Da]	ΔM [ppm]
qTIDNSQGAYQEAFDISK	N-Term(Gln->pyro-Glu)	71	2	1997.9	2.02
QTIDNSQGAYQEAFDISKK		46	3	2143.09	35.1

Licensed MASCOT software (Matrix Science, UK) was used to unambiguously identify proteins from NCBInr sequence database. NanoLC-MS/MS data were searched using a mass tolerance value of 600 ppm for precursor ion and 0.6 Da for MS/MS fragments, trypsin as the proteolytic enzyme, a missed cleavages maximum value of 1, and Cys carbamidomethylation as fixed modification, and pyroglutamate (peptide N-terminal Gln), pyro-carbamidomethyl Cys (peptide N-terminal CAM-Cys) and Met oxidation as variable modifications. Possible charge states +2 and +3. Candidates with almost 2 assigned peptides with an individual MASCOT score > 44 ($p<0.05$) were considered significant. Protein gene names and UniProt codes were reported as well as the sequence and charge state of each peptide used for identification, the MH+ values, and the error expressed in ppm.

SUPPLEMENTARY TABLE 3. List of ATP7B-H1069Q-specific interactors.

PROTEIN	UNIPROT CODE	GENE NAME	# Peptides	MW [kDa]	
1-phosphatidylinositol 4,5-bisphosphate phosphodiesterase gamma-1	**P19174**	**PLCG1**	**3**	**161**	
Peptide Sequences	Modifications	IonScore	Charge	MH+ [Da]	ΔM [ppm]
SGDITYGQFAQLYR		81	2	1618.87	53.60
TmDLPFLEASTLR	M2(Oxidation)	56	2	1510.01	166.00
APLFPAPK		27	2	840.75	280.00
Golgi apparatus protein 1	**Q92896**	**GLG1**	**2**	**134**	
Peptide Sequences	Modifications	IonScore	Charge	MH+ [Da]	ΔM [ppm]
VAELSSDDFHLDR		59	3	1504.01	205.00
IIIQESALDYR		58	2	1320.91	149.00
Integrin beta-1	**P05556**	**ITGB1**	**4**	**88**	
Peptide Sequences	Modifications	IonScore	Charge	MH+ [Da]	ΔM [ppm]
SAVTTVVNPK		67	2	1015.15	-419.41
IGFGSFVEK		37	2	983.67	156.00
LKPEDITQIQPQQLVLR		31	3	2019.52	186.00
SGEPQTFTLK		19	2	1107.65	76.50
T-complex protein 1 subunit beta	**P78371**	**CCT2**	**8**	**57**	
Peptide Sequences	Modifications	IonScore	Charge	MH+ [Da]	ΔM [ppm]
EALLSSAVDHGSDEVK		70	2	1656.77	-21.01
GATQQILDEAER		61	2	1330.67	9.79
HGINCFINR		48	2	1130.67	107.00
QDLmNIAGTTLSSK	M4(Oxidation)	38	2	1494.89	97.70
VLVDMSR		32	2	819.57	163.00
AAHSEGNTTAGLDMR		15	3	1530.77	51.60
ILIANTGMDTDKIK		44	3	1532.92	65.40
NIGVDNPAAK		21	2	998.63	66.40
60S ribosomal protein L18	**Q07020**	**RPL18**	**5**	**18**	
Peptide Sequences	Modifications	IonScore	Charge	MH+ [Da]	ΔM [ppm]
ILTFDQLALDSPK		58	2	1461.01	187.00
TAVVVGTITDDVR		75	2	1345.89	-14.49
GCGTVLLSGPR		52	2	1116.75	152.00
TNSTFNQVVLK		44	2	1250.73	47.00
SQDIYLR		17	2	894.53	72.50
Proteasome activator complex subunit 1	**Q06323**	**PSME1**	**8**	**28**	
Peptide Sequences	Modifications	IonScore	Charge	MH+ [Da]	ΔM [ppm]
TENLLGSYFPK		61	2	1268.91	206.00
IEDGNNFGVAVQEK		77	2	1519.81	101.00
qLVHELDEAEYR	N-Term(Gln->pyro-Glu)	48	2	1484.83	88.40
APLDIPVPDPVKEK		40	3	1518.47	407.00
LmVMEIR	M2(Oxidation)	39	2	907.67	219.00
IVVLLQR		22	2	840.75	222.00
qPHVGDYR	N-Term(Gln->pyro-Glu)	19	2	954.61	178.00
qLVHELDEAEYRDIR	N-Term(Gln->pyro-Glu)	28	3	1869.28	204.00
CALNEXIN	**P27824**	**CANX**	**7**	**71**	
Peptide Sequences	Modifications	IonScore	Charge	MH+ [Da]	ΔM [ppm]
IVDDWANDGWGLK		77	2	1488.87	108.00
APVPTGEVYFADSFDR		67	2	1770.83	-0.36
GTLSGWILSK		53	2	1061.73	126.00
IVDDWANDGWGLKK		46	3	1617.02	135.00
TPYTImFGPDK	M6(Oxidation)	46	2	1285.77	124.00
LPGDKGLVLmSR	M10(Oxidation)	28	3	1301.87	116.00
IPDPEAVKPDDWDEDAPAK		43	3	2108.02	25.40
Aldehyde dehydrogenase X, mitochondrial	**P30837**	**ALDH1B1**	**4**	**57**	
Peptide Sequences	Modifications	IonScore	Charge	MH+ [Da]	ΔM [ppm]
LAPALATGNTVVMK		63	2	1385.95	123.00
IAKEEIFGPVQPLFK		43	3	1716.35	223.00
VAEQTPLSALYLASLIK		86	2	1817.30	149.00
VTLELGGK		31	2	816.51	37.00
T-complex protein 1 subunit epsilon	**P48643**	**CCT5**	**6**	**59.43073302**	
Peptide Sequences	Modifications	IonScore	Charge	MH+ [Da]	ΔM [ppm]
qQISLATQmVR	N-Term(Gln->pyro-Glu); M9(Oxidation)	78	2	1273.75	75.30
IAILTcPFEPPKPK	C6(Carbamidomethyl)	55	3	1611.47	359.00
GVIVDKDFSHPQmPK	M13(Oxidation)	47	3	1714.85	579.00
TSLGPDGLDK		16	2	1002.54	42.40
LMGLEALK		31	2	874.67	190.00
MLVIEQcK	C7(Carbamidomethyl)	28	2	1020.51	-8.74
40S ribosomal protein S21	**P63220**	**RPS21**	**4**	**8**	
Peptide Sequences	Modifications	IonScore	Charge	MH+ [Da]	ΔM [ppm]
MGESDDSILR		66	2	1122.57	38.50
TYAIcGAIR	C5(Carbamidomethyl)	34	2	1024.53	8.12
RMGESDDSILR		28	2	1278.77	127.00

DHASIQmNVAEVDKVTGR	M7(Oxidation)	50	3	1987	526.00
6-phosphogluconate dehydrogenase, decarboxylating	**P52209**	**PGD**	**6**	**50**	
Peptide Sequences	Modifications	IonScore	Charge	MH+ [Da]	ΔM [ppm]
GILFVGSGVSGGEEGAR		88	2	1591.87	41.00
VDDFLANEAK		53	2	1121.67	112.00
TVSKVDDFLANEAK		44	2	1536.87	53.60
AGQAVDDFIEK		41	2	1192.61	23.70
TIFQGIAAK		28	2	948.67	128.00
SFLEDIRK		17	2	1007.07	-476.16
DNA replication licensing factor MCM3	**P25205**	**MCM3**	**6**	**91**	
Peptide Sequences	Modifications	IonScore	Charge	MH+ [Da]	ΔM [ppm]
TPmENIGLQDSLLSR	M3(Oxidation)	93	2	1689.69	-91.70
GDINILLIGDPSVAK		62	2	1524.31	-361.22
GSSGVGLTAAVTTDQETGER		91	2	1935.92	3.77
VALLDVFR		33	2	932.73	189.00
TLETLIR		33	2	845.69	217.00
LIVNVNDLRR		21	3	1211.9	152.00
40S ribosomal protein S27	**P42677**	**RPS27**	**2**	**10**	
Peptide Sequences	Modifications	IonScore	Charge	MH+ [Da]	ΔM [ppm]
LVQSPNSYFmDVK	M10(Oxidation)	72	2	1543.79	30.20
LTEGcSFR	C5(Carbamidomethyl)	31	2	969.51	69.10
Interleukin enhancer-binding factor 3	**Q12906**	**ILF3**	**7**	**75**	
Peptide Sequences	Modifications	IonScore	Charge	MH+ [Da]	ΔM [ppm]
AYAALAALEK		57	2	1020.69	118.00
EDITQSAQHALR		52	2	1368.57	-83.26
VLQDMGLPTGAEGR		50	2	1443.85	87.80
LFPDTPLALDANK		38	2	1414.77	10.70
VLGMDPLPSK		37	2	1056.75	168.00
LNQLKPGLQYK		27	3	1301.63	160.00
LAAFGQLHK		21	2	984.65	91.70
Peptidyl-prolyl cis-trans isomerase FKBP1A	**P62942**	**FKBP1A**	**3**	**12**	
Peptide Sequences	Modifications	IonScore	Charge	MH+ [Da]	ΔM [ppm]
GVQVETISPGDGR		62	2	1314.75	66.90
GWEEGVAQMSVGQR		57	2	1533.73	13.90
GVQVETISPGDGRTFPK		45	3	1788.11	105.00
Heat shock 70 kDa protein 4L	**O95757**	**HSPA4L**	**2**	**97**	
Peptide Sequences	Modifications	IonScore	Charge	MH+ [Da]	ΔM [ppm]
DISTTLNADEAVAR		85	2	1475.73	-0.60
VLATTFDPYLGGR		64	2	1409.95	149.00
Programmed cell death protein 5	**O14737**	**PDCD5**	**3**	**13**	
Peptide Sequences	Modifications	IonScore	Charge	MH+ [Da]	ΔM [ppm]
NSILAQVLDQSAR		84	2	1414.93	119.00
AVENYLIQmAR	M9(Oxidation)	64	2	1323.43	-181.29
LSNLALVKPEK		18	3	1211.93	165.00
tRNA-splicing ligase RtcB homolog	**Q9Y3I0**	**HSPC117**	**4**	**55**	
Peptide Sequences	Modifications	IonScore	Charge	MH+ [Da]	ΔM [ppm]
qIGNVAALPGIVHR	N-Term(Gln->pyro-Glu)	59	2	1428.01	141.00
SYNDELQFLEK		56	2	1385.79	97.10
IASPEGQDYLK		42	2	1220.79	145.00
SSmTFLTR	M3(Oxidation)	29	2	958.53	69.40
Proteasome activator complex subunit 2	**Q9UL46**	**PSME2**	**5**	**27**	
Peptide Sequences	Modifications	IonScore	Charge	MH+ [Da]	ΔM [ppm]
IEDGNDFGVAIQEK		68	2	1534.89	101.00
ALVHERDEAAYGELR		55	3	1729.01	86.30
TKVEAFQTTISK		33	2	1352.85	81.90
cGFLPGNEK	C1(Carbamidomethyl)	29	2	1021.57	93.70
AmVLDLR	M2(Oxidation)	28	2	833.59	166.00
cytochrome c oxidase subunit 5B, mitochondrial precursor	**Q6FHJ9**	**COX5B**	**3**	**14**	
Peptide Sequences	Modifications	IonScore	Charge	MH+ [Da]	ΔM [ppm]
GLDPYNVLAPK		56	2	1186.69	38.90
KGLDPYNVLAPK		47	3	1315.06	254.00
LVPQQLAH		19	2	905.53	13.70
Cytochrome c oxidase subunit 5A, mitochondrial	**P20674**	**COX5A**	**4**	**17**	
Peptide Sequences	Modifications	IonScore	Charge	MH+ [Da]	ΔM [ppm]
GINTLVTYDmVPEPK	M10(Oxidation)	55	2	1692.91	36.30
LNDFASTVR		47	2	1022.59	64.80
ILEVVKDK		34	2	943.67	96.00
RLNDFASTVR		28	2	1178.85	191.00
Elongation factor 1-beta	**P24534**	**EEF1B2**	**2**	**25**	
Peptide Sequences	Modifications	IonScore	Charge	MH+ [Da]	ΔM [ppm]
SPAGLQVLNDYLADK		88	2	1604.13	187.00
SIQADGLVWGSSK		57	2	1347.77	61.20
ATP synthase subunit e, mitochondrial	**P56385**	**ATP5I**	**3**	**8**	
Peptide Sequences	Modifications	IonScore	Charge	MH+ [Da]	ΔM [ppm]
YSALFLGVAYGATR		45	2	1488.21	-384.33
VPPVQVSPLIK		45	2	1176.81	66.00
ELAEDDSILK		44	2	1132.69	106.00

Thioredoxin domain-containing protein 5	Q8NBS9	TXNDC5	5	44	
Peptide Sequences	Modifications	IonScore	Charge	MH+ [Da]	ΔM [ppm]
GYPTLLWFR		46	2	1152.83	185.00
GYPTLLLFR		45	2	1079.79	156.00
FVLSQAKDEL		39	2	1149.85	207.00
EFPGLAGVK		29	2	917.65	157.00
TLAPTWEELSK		18	2	1274.75	70.70
Dihydrolipoyllysine-residue acetyltransferase component of pyruvate dehydrogenase complex, mitochondrial	**P10515**	**DLAT**	**3**	**69**	
Peptide Sequences	Modifications	IonScore	Charge	MH+ [Da]	ΔM [ppm]
GVETIANDVVSLATK		99	2	1516.97	99.60
GIDLTQVK		39	2	873.47	-35.86
ILVPEGTR		17	2	884.59	82.30
28S ribosomal protein S28, mitochondrial	**Q9Y2Q9**	**MRPS28**	**2**	**20**	
Peptide Sequences	Modifications	IonScore	Charge	MH+ [Da]	ΔM [ppm]
NVESFASmLR	M8(Oxidation)	53	2	1169.75	163.00
LLDLELTSR		52	2	1059.832723	216.00
Ubiquitin thioesterase OTUB1	**Q96FW1**	**OTUB1**	**2**	**46**	
Peptide Sequences	Modifications	IonScore	Charge	MH+ [Da]	ΔM [ppm]
IQQEIAVQNPLVSER		68	2	1723.93	-0.57
LLTSGYLQR		41	2	1050.33	-249.13
EH domain-containing protein 4	**Q9H223**	**EHD4**	**3**	**61**	
Peptide Sequences	Modifications	IonScore	Charge	MH+ [Da]	ΔM [ppm]
AGGADAVQTVTGGLR		63	2	1372.77	39.90
SISVIDSPGILSGEK		44	2	1502.25	294.00
EYQISAGDFPEVK		30	2	1482.89	123.00
Acetyl-CoA acetyltransferase, cytosolic	**Q9BWD1**	**ACAT2**	**6**	**41**	
Peptide Sequences	Modifications	IonScore	Charge	MH+ [Da]	ΔM [ppm]
GLIEVKTDEFPR		78	3	1404.02	173.00
VAVLSQNR		40	2	886.79	319.00
ILVTLLHTLER		31	3	1308.14	261.00
VNIEGGAIALGHPLGASGCR		58	3	1949.17	94.1
ELGLNPEK		18	2	899.55	77.30
APHLAYLR		18	2	940.43	-110.22
Fibrinogen gamma chain	**P02679**	**FGG**	**5**	**49**	
Peptide Sequences	Modifications	IonScore	Charge	MH+ [Da]	ΔM [ppm]
YLQEIYNSNNQK		60	2	1513.95	148.00
TSTADYAmFK	M8(Oxidation)	38	2	1150.57	55.90
qSGLYFIKPLK	N-Term(Gln->pyro-Glu)	30	2	1276.89	128.00
VELEDWNGR		21	2	1117.73	184.00
AIQLTYNPDESSKPNmIDAATLK	M16(Oxidation)	61	3	2536.21	-13.59
Alpha-aminoadipic semialdehyde dehydrogenase	**P49419**	**ALDH7A1**	**4**	**54**	
Peptide Sequences	Modifications	IonScore	Charge	MH+ [Da]	ΔM [ppm]
VNLLSFTGSTQVGK		59	2	1451.15	250.00
QGLSSSIFTK		46	2	1067.67	93.40
MIGGPILPSER		33	2	1169.79	135.00
VGNPWDPNVLYGPLHTK		40	3	1907.41	233.00
26S proteasome non-ATPase regulatory subunit 2	**Q13200**	**PSMD2**	**3**	**94**	
Peptide Sequences	Modifications	IonScore	Charge	MH+ [Da]	ΔM [ppm]
VGQAVDVVGQAGKPK		57	3	1453.06	178.00
ELDIMEPKVPDDIYK		34	3	1805.2	173.00
mLVTFDEELRPLPVSVR	M1(Oxidation)	58	3	2018.26	2.37
26S proteasome non-ATPase regulatory subunit 7	**P51665**	**PSMD7**	**2**	**28**	
Peptide Sequences	Modifications	IonScore	Charge	MH+ [Da]	ΔM [ppm]
DIKDTTVGTLSQR		63	2	1433.75	-4.70
SVVALHNLINNK		57	2	1321.87	86.40
E3 UFM1-protein ligase 1 [Homo sapiens]	**O94874**	**UFL1**	**5**	**89**	
Peptide Sequences	Modifications	IonScore	Charge	MH+ [Da]	ΔM [ppm]
FFADDTQAALTK		49	2	1327.17	-361.92
AVFVPDIYSR		32	2	1166.77	131.00
SVFMSSTTSASGTGR		31	2	1475.73	36.10
LAADFQR		22	2	820.47	50.70
TYLEVVR		17	2	879.69	227.00
Protein transport protein Sec61 subunit beta	**P60468**	**SEC61B**	**2**	**10**	
Peptide Sequences	Modifications	IonScore	Charge	MH+ [Da]	ΔM [ppm]
TTSAGTGGMWR		49	2	1124.49	-20.12
FYTEDSPGLK		33	2	1156.65	17.90
26S proteasome non-ATPase regulatory subunit 13	**Q9UNM6**	**PSMD13**	**5**	**35**	
Peptide Sequences	Modifications	IonScore	Charge	MH+ [Da]	ΔM [ppm]
VLDLQQIK		48	2	956.67	99.70
LNIGDLQVTK		44	2	1100.69	56.10
QLTFEEIAK		40	2	1078.79	199.00
QmTDPNVALTFLEK	M2(Oxidation)	22	2	1623.05	150.00
FLGCVDIKDLPVSEQQER		37	3	2133.37	151.00
Small nuclear ribonucleoprotein E	**P62304**	**SNRPE**	**3**	**11**	
Peptide Sequences	Modifications	IonScore	Charge	MH+ [Da]	ΔM [ppm]

VmVQPINLIFR	M2(Oxidation)	53	2	1345.89	94.20
ImLKGDNITLLQSVSN	M2(Oxidation)	38	2	1761.95	6.38
GDNITLLQSVSN		33	2	1260.79	119.00
Nuclear migration protein nudC	**Q9Y266**	**NUDC**	**2**	**38**	
Peptide Sequences	Modifications	IonScore	Charge	MH+ [Da]	ΔM [ppm]
GQPAIIDGELYNEVK		54	2	1645.81	-18.50
LVSSDPEINTK		45	2	1202.75	105.00
Ubiquitin carboxyl-terminal hydrolase isozyme L3	**P15374**	**UCHL3**	**2**	**22**	
Peptide Sequences	Modifications	IonScore	Charge	MH+ [Da]	ΔM [ppm]
FLEESVSMSPEER		52	2	1539.69	-4.42
YLENYDAIR		47	2	1156.79	199.00
Ubiquitin conjugation factor E4 A	**Q14139**	**UBE4A**	**2**	**120**	
Peptide Sequences	Modifications	IonScore	Charge	MH+ [Da]	ΔM [ppm]
SYSPTLFAQTVR		58	2	1369.85	104.00
VFVEYIQPK		37	2	1122.87	226.00
Lymphokine-activated killer T-cell-originated protein kinase	**Q96KB5**	**PBK**	**2**	**36**	
Peptide Sequences	Modifications	IonScore	Charge	MH+ [Da]	ΔM [ppm]
ASQDPFPAAIILK		57	2	1370.91	106.00
SLNDLIEER		44	2	1088.65	86.90
Cystatin-B	**P04080**	**CSTB**	**2**	**11**	
Peptide Sequences	Modifications	IonScore	Charge	MH+ [Da]	ΔM [ppm]
SQVVAGTNYFIK		60	2	1326.83	96.20
AKHDELTYF		21	2	1123.65	98.80
Mitogen-activated protein kinase 14	**Q16539**	**MAPK14**	**2**	**41**	
Peptide Sequences	Modifications	IonScore	Charge	MH+ [Da]	ΔM [ppm]
NYIQSLTQmPK	M9(Oxidation)	48	2	1338.53	-104.26
ILDFGLAR		38	2	904.67	163.00
Asparagine--tRNA ligase, cytoplasmic	**O43776**	**NARS**	**3**	**63**	
Peptide Sequences	Modifications	IonScore	Charge	MH+ [Da]	ΔM [ppm]
IFDSEEILAGYKR		45	3	1540.97	114.00
SPAGSIVHELNPNFQPPK		36	3	1931.15	-436.01
IGALEGYR		31	2	878.67	228.00
Dolichyl-diphosphooligosaccharide--protein glycosyltransferase subunit DAD1	**P61803**	**DAD1**	**2**	**12**	
Peptide Sequences	Modifications	IonScore	Charge	MH+ [Da]	ΔM [ppm]
FLEEYLSSTPQR		48	2	1469.79	44.70
SASVVSVISR		28	2	1005.03	458.00
Nucleophosmin	**P06748**	**NPM1**	**2**	**25**	
Peptide Sequences	Modifications	IonScore	Charge	MH+ [Da]	ΔM [ppm]
GPSSVEDIK		47	2	931.55	85.60
LLSISGKR		11	2	873.47	-90.40
6-phosphofructokinase, liver type	**P17858**	**PFKL**	**3**	**90**	
Peptide Sequences	Modifications	IonScore	Charge	MH+ [Da]	ΔM [ppm]
VFANAPDSAcVIGLK	C10(Carbamidomethyl)	45	2	1561.95	95.10
AIGVLTSGGDAQGmNAAVR	M14(Oxidation)	82	2	1803.92	17.20
IMEVIDAITTTAQSHQR		47	3	1914.35	199.00
Acyl-CoA-binding protein	**P07108**	**DBI**	**2**	**10**	
Peptide Sequences	Modifications	IonScore	Charge	MH+ [Da]	ΔM [ppm]
TKPSDEEmLFIYGHYK	M8(Oxidation)	41	3	1973.96	17.30
QATVGDINTERPGMLDFTGK		48	3	2150.24	88.80
S-methyl-5'-thioadenosine phosphorylase	**Q13126**	**MTAP**	**2**	**32**	
Peptide Sequences	Modifications	IonScore	Charge	MH+ [Da]	ΔM [ppm]
YVDTPFGKPSDALILGK		47	3	1821.29	174.00
IGIIGGTGLDDPEILEGRTEK		46	3	2183.39	110.00
Hsp90 co-chaperone Cdc37	**Q16543**	**CDC37**	**3**	**44**	
Peptide Sequences	Modifications	IonScore	Charge	MH+ [Da]	ΔM [ppm]
ASEAKEGEEAGPGDPLLEAVPK		51	3	2195.3	555.00
EGEEAGPGDPLLEAVPK		28	2	1708.04	123.00
LQAEAQQLR		16	2	1056.74	164.00
Alanine aminotransferase 2	**Q8TD30**	**GPT2**	**3**	**58**	
Peptide Sequences	Modifications	IonScore	Charge	MH+ [Da]	ΔM [ppm]
KPFTEVIR		13	2	989.66	96.00
MTILPPVEK		27	2	1027.68	104.00
ANIGDAQAMGQQPITFLR		68	2	1931.04	37.50

Licensed MASCOT software (Matrix Science, UK) was used to unambiguously identify proteins from NCBInr sequence database. NanoLC-MS/MS data were searched using a mass tolerance value of 600 ppm for precursor ion and 0.6 Da for MS/MS fragments, trypsin as the proteolytic enzyme, a missed cleavages maximum value of 1, and Cys carbamidomethylation as fixed modification, and pyroglutamate (peptide N-terminal Gln), pyro-carbamidomethyl Cys (peptide N-terminal CAM-Cys) and Met oxidation as variable modifications. Possible charge states +2 and +3. Candidates with almost 2 assigned peptides with an individual MASCOT score > 44 (p<0.05) were considered significant. Protein gene names and UniProt codes were reported as well as the sequence and charge state of each peptide used for identification, the MH+ values, and the error expressed in ppm.

SUPPLEMENTARY MATERIALS AND METHODS

Antibodies, Reagents, DNAs and Adenoviruses

The following antibodies were used. Anti-α-tubulin was from Sigma-Aldrich (St. Louis, USA), anti-TGN46 from AbD Serotec (Oxford, UK), anti-MRP2 from Enzo Life Sciences (Lausen, Switzerland), anti-GM130, anti-giantin and anti-GFP from Abcam (Cambridge, UK), phospho-p38, phospho-JNK, phosphor-ERK, p38, JNK and ERK (Cell Signaling Techology, Beverly MA USA) anti- secondary Alexa Fluor 488, 568, 633, 647-conjugated antibodies were from Invitrogen-Life Technologies (Grand Island, USA), secondary peroxidase conjugate antibodies were from Calbiochem (Darmstadt, Germany). GoldEnhance™ EM kit and 1.4nm gold-conjugated Fab' fragment of anti-rabbit IgGs were from Nanoprobes (Yaphank, NY 11980-9710, USA). The DNAs of GFP-tagged ATP7B and ATP7B^{H1069Q} were provided by Svetlana Lutsenko (John Hopkins Medical School, Baltimore, MD, USA) and by Dominik Huster (University of Leipzig, Leipzig, Germany). The cDNAs of transcription-based luciferase reporter (pGL3-E1b-TATA-4MRE) as well as DNAs of ATP7A and its mutants were reported before (13). DNAs of flag-tagged MKK3, 4, 6 and 7 were obtained from Addgene (Cambridge MA, USA). To obtain the R778L, D765N, L776V, A874V and L1083F mutants of ATP7B, the pEGFPC1-ATP7B construct was used as a template, and site-direct mutagenesis was performed according to the manufacturer instructions for site-directed mutagenesis using the QuickChange kit (Stratagene, La Jolla, CA, USA). Recombinant adenoviruses containing ATP7B-GFP or ATP7B^{H1069Q}-GFP were reported before (14).

Cell culture and Treatments

HeLa, HepG2 cells and primary mouse hepatocytes were grown in Dulbecco's Modified Eagle's medium (DMEM) supplemented with FCS 10% (decomplemented for HepG2 cells), L-glutamine and Penicillin/Streptomycin. HeLa, HepG2 cells and primary

hepatocytes were treated with 200 μM Cu-chelating agent BCS overnight or with 100-200 μM $CuSO_4$ in culture medium at 37°C for 2 or 8 h. To inhibit p38 or JNK specific inhibitors SB202190 (Sigma Aldrich, USA) or SP600125 (Sigma Aldrich, USA) were used respectively. To inhibit protein biosynthesis Cycloheximide (Sigma Aldrich, USA) 100 μg/mL was used at 2,4 and 6 hours. To inhibit the proteasome MG132 (Sigma) 20μM for 4 hours was used.

Adenoviral Infection, DNA Transfection, RNA interference, RNA Preparation and Q-PCR

HeLa and HepG2 cells were infected with first generation adenovirus containing ATP7B-GFP or ATP7B^{H1069Q}-GFP respectively with a multiplicity of infection (MOI) of 50 and 200 virus particles per cell respectively. HepG2 or HeLa cells were transiently transfected with jetPEI TM-Hepatocyte or Trans IT LT1 Transfection transfection reagents (Polyplus transfection, New York NY USA) respectively. siRNAs targeting MAPK8, MAPK9, MAPK10, MAPK11, MAPK12, MAPK13, MAPK14, MAP3K11 were purchased from Sigma-Aldrich and transfected using Oligofectamine (Invitrogen, Carlsbad USA). Total RNAs from control cells and silenced HeLa cells were purified with the using QIA shredder and extracted with RNeasy Protect Mini Kit. Total RNA was converted into cDNA with QuantiTect Reverse Transcription kit. Q-PCR experiments were performed using Light Cycler 480 Syber Green MasterMix for cDNA amplification and in LightCycler 480 II for signal detection. Q-PCR results were analyzed using the comparative Ct method normalized against housekeeping gene β-Actin.

VSVG trafficking assay.

To evaluate the impact of p38 and JNK inhibitors on overall membrane trafficking thermo-sensitive form of vesicular stomatitis virus glycoprotein fused with GFP (VSVG-GFP) was transfected into HeLa cells. Control and inhibitor-treated cells were incubated at 40°C to accumulate VSVG in the ER. Then the temperature was shifted to 32°C to activate VSVG-GFP trafficking. Cells were fixed at different time intervals after the temperature shift and analyzed using confocal microscopy.

Immunofluorescence

Cells were fixed for 10 min with 4% paraformaldehyde (PFA) in 0.2 M HEPES followed by incubation with blocking/permeabilizing solution: 0.5% bovine serum albumin (BSA), 0.1% saponin, 50 mM NH_4Cl in PBS for 20-30 min. Primary and secondary antibodies were diluted in blocking/permeabilizing solution and added to the cells for 1h/overnight or 45 min respectively. Samples were examined with a ZEISS LSM 700 or LSM 710 confocal microscopes equipped with a 63X 1.4 NA oil objective.

For fluorescent Cu detection with CS3 cells were incubated with 5 μM CS3 (kindly provided by Christopher Chang, Berkeley USA) for 15 min at 37°C. CS3 was excited with 561 nm laser of LSM710 and its emission was collected from 565 to 650 nm. Co-localization module of ZEISS ZEN 2008 software was used to measure co-localization of ATP7B with different intracellular markers. ATP7B fluorescent signal inside canalicular domains and CS3 cytosolic and canalicular surface signals were measured using ZEISS ZEN 2008 software and reported in arbitrary units (au).

Fluorescent recovery after photobleaching (FRAP)

Time-lapse sequences from control and inhibitor-treated HeLa cells expressing $ATP7B^{H1069Q}$-GFP were taken at ZEISS LSM 700 or LSM 710 confocal stages at 37°C. Digital images were collected at 3-second intervals. Selective photobleaching of GFP in the Golgi regions was carried out using 100 consecutive scans with a 488 nm laser line at full power. Average fluorescence intensities and $t_{1/2}$ of the recovery in the Golgi regions were quantified using FRAP module of ZEISS ZEN 2008 software.

Western blot analysis

Cells were then solubilized in RIPA buffer. The protein concentration in each sample was evaluated using Bradford Protein Assay. Proteins were eluted with SDS sample buffer and analyzed by immunoblot analysis. Antibodies against GFP, tubulin, phospho-p38, phospho-JNK, p38 and JNK were used.

Immunoprecipitation and mass spectrometry analysis

To identify the effects of ATP7B ^{H1069Q} overexpression on the proteome of liver cell line, proteomics analysis was performed. For the analysis of the hepatocytes overexpressing ATP7B^{H1069Q}-GFP or ATP7B^{WT}-GFP, cell lysates were incubated with the anti-GFP antibody. Then protein G sepharose beads (Sigma, St Louis, MO, USA) were added to each specimen and immune complexes were collected by centrifugation. The beads were then washed and immunoprecipitated proteins were eluted. The eluted proteins were precipitated in methanol/chloroform and then separated by SDS-PAGE. The gel was stained with Coomassie blue. Protein bands were excised from the gel, and digested with trypsin. Peptide mixtures extracted from the gel were analyzed by nano-chromatography tandem mass spectrometry (nanoLC–MS/MS) on a CHIP MS Ion Trap XCT Ultra equipped with a capillary 1100 HPLC system and a chip cube (Agilent Technologies, Palo Alto, CA). Peptide analysis was performed using data-dependent acquisition of one MS scan (mass range from 400 to 2000 m/z) followed by MS/MS scans of the three most abundant ions in each MS scan. Raw data from nanoLC–MS/MS analyses were employed to query a nonredundant protein database using in house MASCOT software (Matrix Science, Boston, USA).

Subcellular fractionation

To determine the amount of ATP7B protein in in different cellular compartments HepG2 expressing ATP7B^{WT}-GFP or ATP7B^{H1069Q}-GFP (control and treated with p38 or JNK inhibitors) were subjected to subcellular fractionation as described in Balch et al (1984). Cells homogenates were separated using discontinuous sucrose density gradient centrifugation. Fractions were collected at in 1.5 ml tubes by aspiration from the bottom, through a capillary tube attached to a polyethylene tube connected to a peristaltic pump and a fraction collector (total of 14 fractions – ~850 µl each). GM130 was used as marker of the Golgi, PDI of the ER and Sodium/Potassium ATPase of plasma membrane. Amonts of GM130, PDI, Na/K-ATPase and ATP7B were revealed in each fractions by Western blot. Briefly, 90 µl of each fraction was mixed with reducing buffer and boiled for 5 min. Samples were loaded in 10% BIS-TRIS gels and run under denaturing conditions. Gels were transferred to nitrocellulose membranes blocked with 1% BSA and

icubated with antibodies against GM130, GFP, PDI or Na/K-ATPase. Anti-rabbit and anti-mouse HRP-conjugated antibodies were used to reveal primary antibodies.

Copper detection by Inductively Coupled Plasma-Mass Spectrometry (ICP-MS)

To determine intracellular Cu concentrations, cell pellets were lysed. The protein concentration in each sample was evaluated using Bradford Protein Assay (BioRad, Segrate, Italy). Cu concentration in the cell lysates was analyzed by ICP-MS. An aliquot of each sample was diluted 1:10 v/v with 5% HNO_3 and analyzed with an Agilent 7700 ICP-MS (Agilent Technologies, Santa Clara, CA, USA) All values of Cu concentration were normalized for protein content in corresponding cell lysates.

Microarray Analysis

To identify the effects of $ATP7B^{H1069Q}$ expression on the transcriptome, total RNA was extracted from HepG2 cells (expressing either $ATP7B^{H1069Q}$-GFP or $ATP7B^{WT}$-GFP) and hybridized on Affymetrix GeneChips. All of the raw microarray data was formatted for 'Gene Expression Omnibus' (GEO) (http://www.ncbi.mln.nih.gov/geo) to comply with Minimum Information About a Microarray Experiment (MIAME) and Microarray Gene Expression Database (MGED) group standards (GEO number GSE51818). The genes differentially expressed in $ATP7B^{H1069Q}$ expressing cells are listed in Supplementary Table 1. Microarray analyses were carried out with R, a free software environment (available at http://www.r-project.org). After quantification of gene expression with robust multi-array normalization (using the BioConductor package affy http://www.bioconductor.org) the significance of the differential gene expression was determined by computing moderated t-statistic s and false discovery rates with the Limma package. Annotation was based on the genome version from the National Center for Biotechnology Information. The p values obtained were corrected for multiple testing by calculating the estimated false discovery rates using the method of Benjamini-Hochberg. Basal and luminal genes that passed all of the described filtering criteria (including the fold-change cut-off) were entered into the Gene Functional Annotation Tool that is available at the Database for Annotation Visualization and Integrated Discovery (DAVID) website (http://david.abcc.ncifcrf.gov) using their official gene

symbols. The gene ontology options GOTERM_BP_ALL and GOTERM_MF_ALL were selected and a functional annotation chart was generated. A maximum p value of 0.05 was chosen to select only the significant categories.

Luciferase Assay

HeLa cells were plated in a 12-well plate and transfected with pGL3-E1b-TATA-4MRE reporter, empty vector (pEGFP-C1), $ATP7B^{WT}$-GFP or $ATP7B^{H1069Q}$-GFP. After 24 hours, cells were treated with 200 μM $CuSO_4$ for 24 hours. Cells were subsequently harvested in a Passive Lysis Buffer (Promega) according to the manufacturer's instructions. Firefly luciferase and *Renilla* luciferase activities were measured with a Dual-Luciferase® reporter assay system (Promega) on a GloMax® 96 Microplate Luminometer (Promega) according to the manufacturer's instructions. Relative Light Units were calculated by dividing firefly measurements by *Renilla* measurements. All values were normalized to the ATP7B expression levels in the respective specimens and an empty vector was used as a control.

Immuno-electron microscopy.

For pre-embedding immuno-electron cells microscopy were fixed with mixture of 4%PFA and 0.05% glutaraldehyde in 0.2 M HEPES for 15 min and with 4%PFA alone for 30 min, followed by incubation with blocking/permeabilizing solution: 0.5% bovine serum albumin (BSA), 0.1% saponin, 50 mM NH_4Cl in PBS for 20-30 min. Primary anti-GFP antibody and 1.4nm gold-conjugated Fab' fragment of anti-rabbit IgGs were diluted in blocking/permeabilizing solution and added to the cells overnight or for 2h respectively. GoldEnhance™ EM kit was used to enhance ultrasmall gold particles. Then cells were scraped, pelleted, post-fixed in OsO_4 and uranyl acetate and embedded in Epon. For cryo immuno-electron microscopy HepG2 cells or small 1 mm^3 pieces of liver tissue from sacrificed mice were rapidly washed in PBS 1X and fixed immediately with a mixture of 2% freshly prepared paraformaldehyde and 0.2% glutaraldehyde in 0.1 M phosphate buffer for 2 h at room temperature. Before freezing in liquid nitrogen cell and tissue gelatin blocks were immersed in 2.3 M sucrose. From each sample, thin plastic or cryo sections were cut using Leica EM UC7 or Leica EM FC7 ultramicrotomes

respectively (Leica Mycrosystems, Vienna, Austria). Cryo sections were double labeled with antibodies against LAMP1 and GFP. EM images were acquired from thin sections using a FEI Tecnai-12 electron microscope (FEI, Eindhoven, Netherlands) equipped with a VELETTA CCD digital camera (Soft Imaging Systems GmbH, Munster, Germany). Morphometric analysis of lysosomal size, distance between lysosomes and PM, distribution of ATP7B among different intacellular compartments was performed using iTEM software (Olympus SYS, Germany).

Statistical analyses

Data were expressed as mean values ± standard deviation. Statistical significance (t-test) was computed using GraphPad Prism6 software. A p-value <0.05 was considered statistically significant. In all figures * means p-value <0.05, ** p-value <0.01, *** p-value <0.001.